UNIVERSITY OF CALIFORNIA
Merced

Analytical and experimental study of a liquid desiccant heat and mass exchanger operating near water freezing temperature

A Thesis submitted in partial satisfaction
of the requirements for the degree of

Master of Science

in

Mechanical Engineering

by

Sergio M. Pineda

Committee in Charge:

Professor Carlos Coimbra, Chair

Professor Gerardo Diaz

Professor Roland Winston

May 2009

The Thesis of

Sergio M. Pineda is approved:

_____

Professor Gerardo Diaz

_____

Professor Roland Winston

_____

Professor Carlos Coimbra, Committee Chair

April 2009

Analytical and experimental study of a liquid desiccant heat and mass exchanger operating near water freezing temperature

by

Sergio M. Pineda

To my family and to the importance of

being.

Acknowledgements

I wish to express my sincere gratitude to my advisor, Prof. Gerardo Diaz, for his continuous support, encouragement, and patience which made this thesis possible, and for his endurance in correcting both my scientific and stylistic errors. I would like to express my sincere appreciations to the members of the thesis committee, Prof. Roland Winston and Prof. Carlos Coimbra, for their suggestions towards improving the quality of my research experience. I would also like to thank Lynnette Ramirez for the valuable discussions and efforts at different stages of my research. I wish to give a posthumous acknowledgement to Norma De la Torre for her hard work at UC Merced. Also, I would like to state my deepest love and respect to my wife Sandra and sons Juan and Manuel for their prayers, patience, and support throughout this process. I wish to thanks to Aslan Cold Storage LLC and Del Monte Foods at Kingsburg, Central Valley of California. I would like to convey special thanks to California Energy Commission CEC, because this project was developed under the frame of contract number 500-02-004, WA# MR-062 between the California Energy Commission and the Regents of the University of California.

Curriculum Vitæ

Sergio M. Pineda

Education

2000	Bachelor of Civil Engineering, Universidad Industrial de Santander, Colombia.

Experience

2006 – 2008	Graduate Research Assistant, University of California, Merced.
2000 – 2005	Graduate Research Assistant, UIS, Colombia.

Abstract

Analytical and experimental study of a liquid desiccant heat and mass exchanger operating near water freezing temperature

Sergio M. Pineda

With the rising costs of electricity due to increasing demand of electric power, liquid desiccant systems have received significant attention as a way to reduce latent loads on air conditioning systems. In particular, the performance of liquid desiccant systems in humid climates has shown significant reductions in energy consumption. In general, these liquid desiccant systems are composed by an absorber or dehumidifier and a regenerator that utilizes a heat source to reject the water from the diluted liquid desiccant. As the humidity of the air is absorbed at the dehumidifier, the temperature of the liquid desiccant increases due to the addition of heat from the enthalpy of condensation of the water vapor. Thus, many designs of liquid desiccant absorbers include the flow of a cooling fluid that removes heat from the liquid desiccant lowering its temperature.

A different application of liquid desiccant systems corresponds to the localized removal of moisture from the air inside low temperature rooms that contain relatively high levels of humidity such as refrigerated warehouses for the food industry. The purpose is to reduce the formation of ice at the surface of the evaporator.

Due to the low temperature of the air inside these rooms, no cooling fluid is necessary for the removal of heat from the liquid desiccant. Thus, the designs of the absorbers differ from the designs used in more conventional applications.

In this thesis, mathematical models of the heat and mass transfer for an adiabatic parallel-plate absorber for which a thin film of liquid desiccant flows down its walls and dehumidifies the air in cross-flow configuration are developed. Numerical results are obtained and the performance of the absorber as a function of several parameters including inlet air temperature and relative humidity, inlet liquid desiccant temperature, mass flow rates of air and liquid desiccant, and liquid desiccant concentration is analyzed. The results are compared with experimental data available for an absorber using calcium chloride as the liquid desiccant. The geometry of the absorber is optimized to improve the dehumidifying performance of the core.

Contents

List of Figures

List of Tables

Nomenclature

C	concentration of liquid desiccant (kg_w/kg_{sol})
Cc	calcium chloride concentration in the desiccant film (kg_{CaCl_2}/kg_{sol})
Cp	specific heat capacity capacity at constant pressure (J/kgK)
D	diffusion coefficient ($m2/s$)
fs	cavity width or wall spacing (m)
g	gravitational acceleration (m/s^2)
H	wall height (m)
h_{gf}	latent heat of condensation (J/kg)
k	thermal conductivity (W/m^2K)
L	wall width (m)
Le	Lewis number
$\dot{m}$	mass flow rate (kg/s)
Nu	Nusselt number
p	pressure (Pa)
p_v	vapor pressure (Pa)
p_{v,H_2O}	water vapor pressure (Pa)
Pe	Peclet number
Pr	Prandtl number

Re	Reynolds number
Sh	Sherwood number
Sc	Schmidt number
T	temperature (K)
U	nondimensional velocity in the $x-$direction
u	velocity in the $x-$direction (m/s)
$\vec{V}$	total velocity (m/s)
V	nondimensional velocity in the $y-$direction
v	velocity in the $y-$direction (m/s)
W	humidity ratio of the air (kg_w/kg_{da})
X	nondimensional $x-$coordinate
x	$x-$coordinate
Y	nondimensional $y-$coordinate
y	$y-$coordinate
z	$z-$coordinate

Greek Letters

α	thermal diffusivity (m^2/s)
δ	subdomain thickness (m)

μ	dynamic viscosity ($Pa\ s$)
ν	kinematic viscosity (m^2/s)
τ	shear stress (N/m^2)
ρ	density (kg/m^3)
ω	humidity ratio (kg_w/kg_{da})
Δ	diference operator
Θ	normalized temperature
Λ	normalized concentration

Subscripts and superscripts

a	air subdomain
avg	air subdomain
i	initial condition
int	interfacial region
l	liquid desiccant subdomain
m	mass
me	mean value
w	water species
wb	water bulk

Chapter 1

Introduction

1.1 Motivation

The projection of the world's market energy consumption published by the Energy Information Administration (EIA), predicts an increase in the demand of energy of approximately 50 percent from 2005 to 2030, equivalent to an increase from 487.4 quadrillion kJ (462 quadrillion Btu)

to 733.3 quadrillion kJ (695 quadrillion Btu) [1]. In this context, the demand of energy consumption in countries that are members of the Organization for Economic Cooperation and Development (OECD) is projected to increase by 19 percent during this period, compared to an increase of 85 percent in the non-

OECD countries. This is mostly due to the fact that non-OECD nations such as China and India have a strong projected economic growth.

Fossil fuels such as petroleum, natural gas and coal will remain as the main supply of the energy used worldwide until 2030. Consequently, in response to this high demand for energy, and because of the concentration of oil production within a small group of countries, oil prices are expected to remain relatively high [2]. Furthermore, the increase of fossil fuel usage in the absence of national policies and/or binding of international agreements that limit or reduce greenhouse gas emissions in the reference scenario, will result in the increase of emissions from 28.1 billion metric tons in 2005 to 42.3 billion metric tons in 2030 [1]. Thus, policies that encourage more efficient use and production of energy are required. For example, the efficient use of electricity in industrial applications such as lighting, air conditioning, appliances and industrial motors has a potential impact of 30 percent reduction of emissions [2].

The efficient use of electricity together with innovative technologies are fundamental tools for reaching suitable levels of energy consumption. This technological change translates to an investment that could have a short payback period if adequate policies are developed before 2015 [1]. Locally, the California Energy Commission (CEC) has been stimulating the use of new technologies in several applications. One example is refrigerated warehouses where the energy consump-

tion is clearly intensive and where a large potential for additional energy saving exists [3, 4].

1.2 Structure of the thesis

Chapter 2 presents the definitions of fundamental concepts about liquid desiccant systems (LDS) [5, 6, 7]. Current and proposed computational/physical models, as well as a review of the literature are also presented, together with a summary of materials and technologies of manipulation. Chapter 3 provides a description of the semi-hybrid system with a dehumidification device. Chapter 4 presents a description of the facilities where a liquid desiccant system was designed, built and tested. In Chapter 5, analytical and computational models that simulate the behavior of the absorber in the LDS, relating theoretical analysis with the physical phenomena are presented. Chapter 6 discusses the results from both the predictive model and the physical model that was implemented. Finally, Chapter 7 is dedicated to the conclusions, recomendations and future work for the project.

1.3 Research objective

This work contributes to the evaluation process of technologies for the reduction of water and energy consumption in refrigerated warehouses in the Central Valley of California by testing a semi-hybrid VAC-LDS system.

Through the implementation of a test bed coupled with the development of mathematical models, it is expected to investigate the applicability of the liquid desiccant systems (LDS) technology to the reduction of water consumption, specifically, in the dehumidification process by studying the simultaneous exchange of heat and mass within an absorber device.

- To understand the absorption process driven by vapor pressure difference at the interface between a falling film and air flux under low temperature conditions.

- To generate realistic numerical models that allow the study of the behavior of the falling film, when it undergoes humidity interchange in several geometric configurations.

Chapter 2

Literature survey

2.1 Traditional HVAC and desiccant systems

A regular cold storage or refrigerated warehouse works as a traditional vapor −compression refrigeration cycle (shown in Fig. 2.1). The cycle works using the latent heat of the refrigerant at low pressure and temperature to absorb heat from the air passing through the evaporator and rejecting it to the ambient by means of condensing the refrigerant at high pressure/high temperature at the condenser. Sensible and latent heat are removed from the air going through the evaporators. Energy savings of up to 80 % when the latent load constitutes 90 % of the total cooling load, have been reported with a hybrid desiccant cooling system comprised

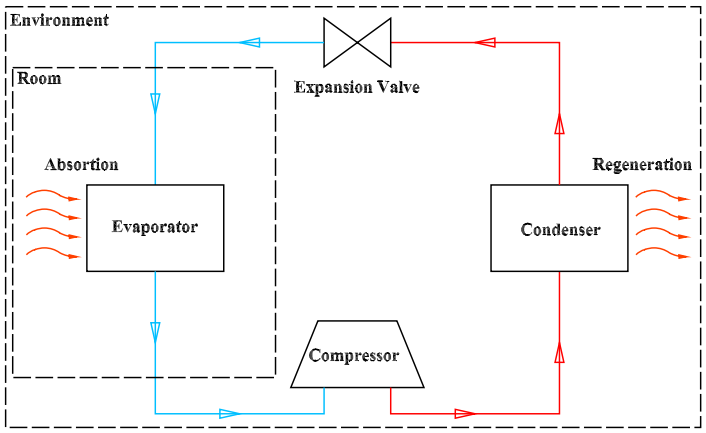

Figure 2.1: Refrigeration cycle

by the traditional vapor compression air conditioning system coupled with a liquid desiccant dehumidifier regenerated by solar energy [8].

A literature review of the theoretical and physical models for a refrigerated warehouse, comparisons between a traditional vapor- compression cycle and a liquid desiccant refrigeration cycle were found [12, 9], where an improved design showed 18 to 23 percent higher coefficient of performance depending on the behavior of *a*) the dehumidifier or regenerator, *b*) the desiccant used for the specific ambient conditions [10, 11], and *c*) the effectiveness of the heat exchanger [12].

Desiccants are natural or synthetic substances capable of absorbing or adsorbing water vapor due to the difference of water vapor pressure between the surrounding air and the desiccant surface. They are hygroscopic at low temperatures (absorb water), but hydrophobic at higher temperatures (reject water). Also, they are encountered in both liquid and solid states. Each liquid and solid desiccant system

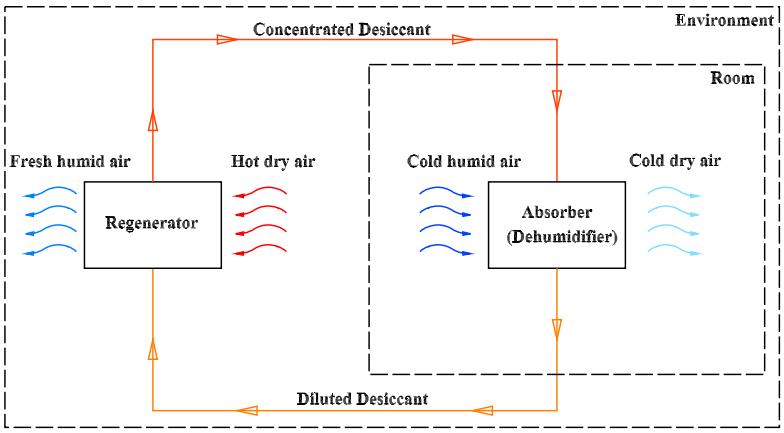

Figure 2.2: Absortion - regeneration cycle

has its own advantages and shortcomings. In addition to having lower regeneration temperature and flexibility in utilization, liquid desiccants have lower pressure drop on the air side. Commonly used desiccant materials and substances include: lithium chloride, calcium chloride, triethylene glycol, silica gels, aluminum silicates (zeolites or molecular sieves), aluminum oxides, lithium bromide and lithium chloride in solution with water [12].

Liquid desiccants are often sprayed into air streams or wetted onto contact surfaces to absorb water vapor from the incoming air (absorption process). The water vapor sorption must be driven out of the desiccant material (regeneration process) so that it can be concentrated enough to absorb water vapor in the next cycle [12, 11, 13, 14]. The complete cycle is shown in Fig. 2.2.

Jain and Bansal [15] evaluate packed-bed dehumidifiers for three commonly used desiccant materials: triethylene glycol (also evaluated in [16]), lithium chloride,

and calcium chloride. The analysis shows wide variations in effectiveness values ranging from 10 percent to 50 percent or more, with higher deviations occurring for lower ratios of liquid to gas flow rates. Kinsara, et. al [17] conducted a simulation study on a desiccant cooling system using an aqueous solution of calcium chloride ($CaCl_2$) as the liquid desiccant. The impact of certain parameters on the system's performance was studied. Those parameters included the desiccant solution inlet temperature, the space sensible heat ratio (SHR), the heat exchanger effectiveness, and the ratio of liquid desiccant flow rate to the air flow rate ($\dot{m}_l/\dot{m}_l$).

In the air conditioning systems field, the use of liquid desiccant systems has become more popular in the past decades [18, 19, 12, 20, 21] due to the necessity of reduction in the consumption of energy and water [9, 15]. The capability of these systems of handling latent heat in the space that will be conditioned by a dehumidifying process, also allows control of the humidity without the overcool/reheat scheme as is done in a regular Ventilating and Air Conditioning system (VAC) [22].

When a liquid desiccant is employed, the dehumidifier (absorber) is located upstream of the evaporators to perform a localized removal of the moisture content of air, with possible configurations including: finned−tube surface, coil−type absorber, spray towers, and packed towers [12, 23].

Most of the studies of the performance of these systems use empirical correlations for dehumidification effectiveness [15]. However, performance also depends on the configuration of the flow between the humid air and the liquid desiccant, and can be classified into parallel flow, counter flow and cross flow [10, 24]. Also, the geometry of the ducts and walls where the liquid desiccant flows has an important effect. A variety of geometrical configurations have been studied in the past. For instance, a parallel plate liquid desiccant system is introduced in Mesquita [25] and a falling film tubular absorber with a falling film regenerator is presented by Jain [23]. Khan and Martinez [26] undertook the study of a mathematical model of a liquid desiccant absorber (dehumidifier) which showed increased performance in terms of the number of transfer units (NTU) of heat transfer between the air flow and the desiccant solution.

A few analytical models are presented in [10, 11] and numerical models in [9, 25, 27], where some works include experimental data [9, 10] from regular prismatic geometries [28] or for several geometric configurations [27, 29].

The systems are usually composed of three components: the regeneration heat source, the dehumidifier (desiccant material), and the cooling unit [12, 15, 30]. In the present study, the behavior of the absorber or dehumidifier device is analyzed under low temperature operating conditions.

2.2 Policies and codes for cold storages

The American Society of Heating, Refrigerating, and Air-Conditioning Engineers (ASHRAE) and the American National Standard Institute (ANSI) have been working together to produce standards such as the Safety Code for Mechanical Refrigeration (15-1994) and the Safety Standard for Refrigeration Systems (15-2001), which have been considered for this work [31, 32, 33]. Moreover, other entities like the Northwest Energy Efficiency Alliance (NEEA) have conducted a study on the application of evaporator fan for refrigerated warehouses.

In California most of the energy efficient programs concerning refrigerated warehouses have been developed by Investor-Owned Utilities (IOUs), until February (2007) when the California Energy Commission published the document Codes and Standards Enhancement Initiative (CASE). The regulation of energy consumption has resulted in a number of initiatives targeting energy efficiency and reduction of consumption. For instance, real-time pricing (RTP), intends to obtain cost savings for the customer if demand can be reduced during hours of high prices and shifted to hours of lower prices.

This project was developed under the frame of contract number 500-02-004, WA# MR-062 between the California Energy Commission and the Regents of the University of California. The development was performed by UC Merced researchers

and a number of companies associated to this initiative(California Energy Commission CEC, Del Monte Foods, Aslan Cold Storage LLC, AIL Research Inc., California Controlled Atmosphere CALCA, Bridgeover Inc., CIEE).

Chapter 3

Description of the problem

High levels of humidity at a warehouse generate water condensation on the evaporator coil, thus forming ice at the coil surface. Consequently, a defrosting cycle needs to be performed once or twice a day. An alternative to this cycle is to use LDS to absorb the excess of moisture that exists in a cold storage area, before the moisture reaches the surface of the evaporator.

In order to test the performance of a desiccant system, a refrigerated room that is cooled by a traditional vapor-compression system was selected. A liquid desiccant system was installed inside Aslan Cold Storage LLC in Kingsburg, CA. as shown in Fig. 3.1. The objetive was to understand the behavior of the absorber in the liquid desiccant system, as it removes humidity from the air inside the room, thus

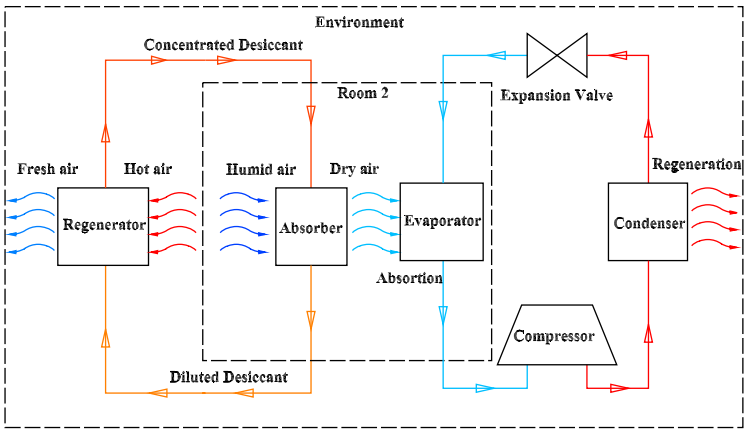

Figure 3.1: Absortion and regeneration cycles

delaying or eliminating ice formation and, consequently, decreasing the water and energy consumption by reducing the number of defrosting cycles.

The absorber core uses calcium chloride as the liquid desiccant and is located inside the warehouse with a suitable set of sensors that record its behavior under a variety of operating conditions. The calcium chloride is brought from a storage tank of approximately $1.14m^3$ (300 gallons) of capacity towards an internal heat exchanger, by means of a hydraulic pump. There, the desiccant is cooled at the internal heat exchanger (IHX) by the flow of desiccant coming from the absorber. The outlet of the high-pressure side of the IHX feeds into the inlet of the absorber. Inside the absorber, the liquid falls as a film down the walls. The liquid desiccant film interacts with the air flow in a cross-flow configuration. The air speed can be adjusted with a simple speed controller connected to the fan. Heat and mass are exchanged at the interface between the air and the liquid desiccant film. The

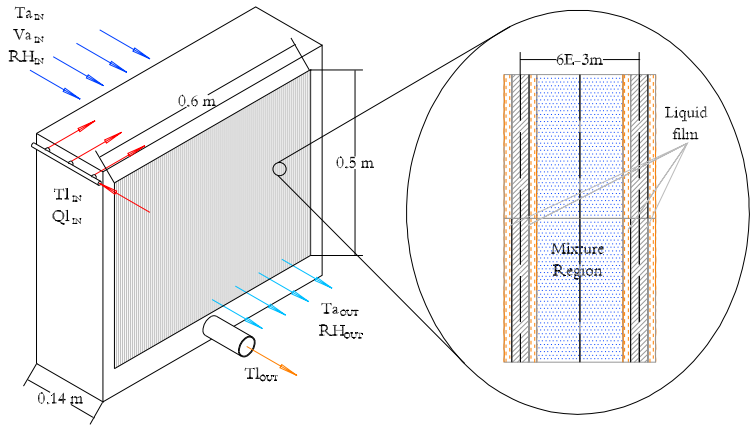

Figure 3.2: General dimensions for the absorber device

dehumidified air goes towards the room and the diluted calcium chloride goes back to the tank to be regenerated.

General characteristics of this device and the location of the sensors are presented in Fig. 3.2 and 3.3, respectively. A more detailed description, including all the components of the liquid desiccant system and the description of the experiment is presented in the following chapter.

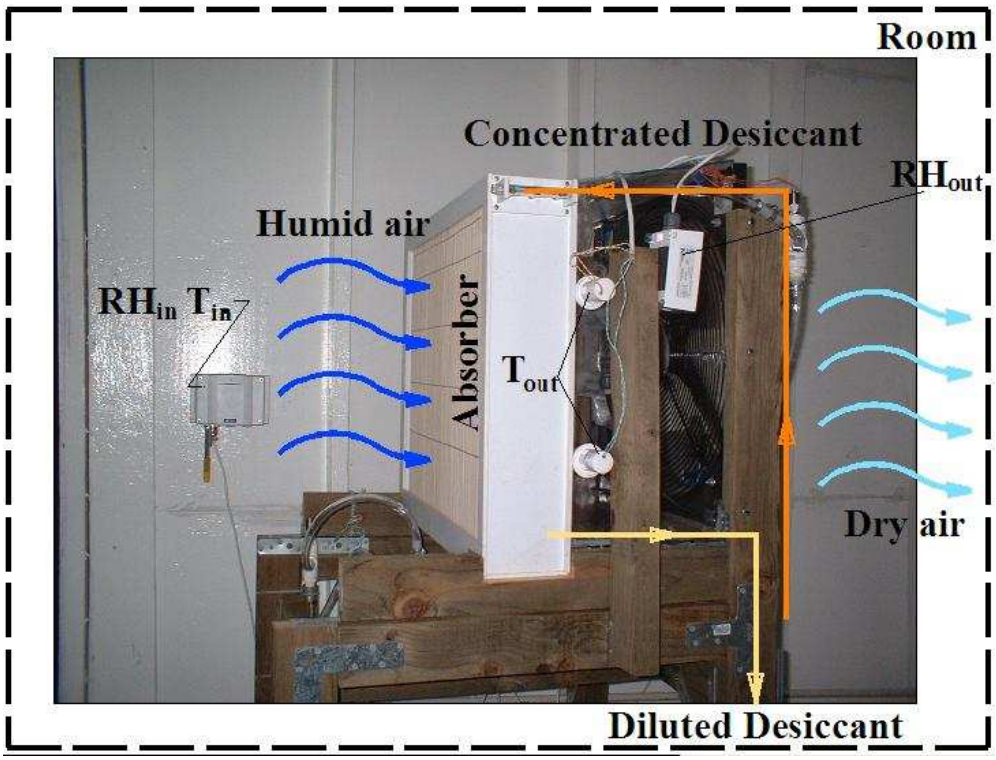

Figure 3.3: Experimental absorber apparatus with its sensors

Chapter 4

Experimental setup and Measurements

4.1 Description of the facilities

The purpose of this section is to describe the site selected for this project as well as the devices that have been placed to obtain measurements of the liquid desiccant system under operating conditions. Aslan Cold Storage, LLC, located at 1045 Simpson Street, Kingsburg, California, about 20 miles south of Fresno, is the site selected as the test facility for the absorber device (see Fig. 4.1).
Within this facility five refrigerated rooms are used for short or long term cold storage of produce. Room 2, is a 25 x 13 m^2 (83 x 41 ft^2) room with six $0.94m.$(37")

Figure 4.1: Location of the facility. Source: Mapquest

diameter fans that use $7457W$ $(10hp)$ Baldor Standard-E motor each. The fans draw air from the room through an opening at the bottom of the bunker wall and through two ammonia evaporators that are located behind the wall, discharging the cooled air into the upper section of the room. A combination of forced convection (from the fans) and natural convection (from density differences) distribute the cooled air throughout the room. The surface area of each evaporator (ammonia coil) is approximately 4.6 x 1.2 m^2 (15 x 4 ft^2) and the design velocity of the air at the surface of the coils is approximately $3.05m/s$ $(600fpm)$ (varies by season). Consequently, the design air flow is $34m^3/s$ $(72,000cfm)$. The air temperature inside the room is kept between 2 and 12^oC $(35.6 - 53.6^oF)$ and the

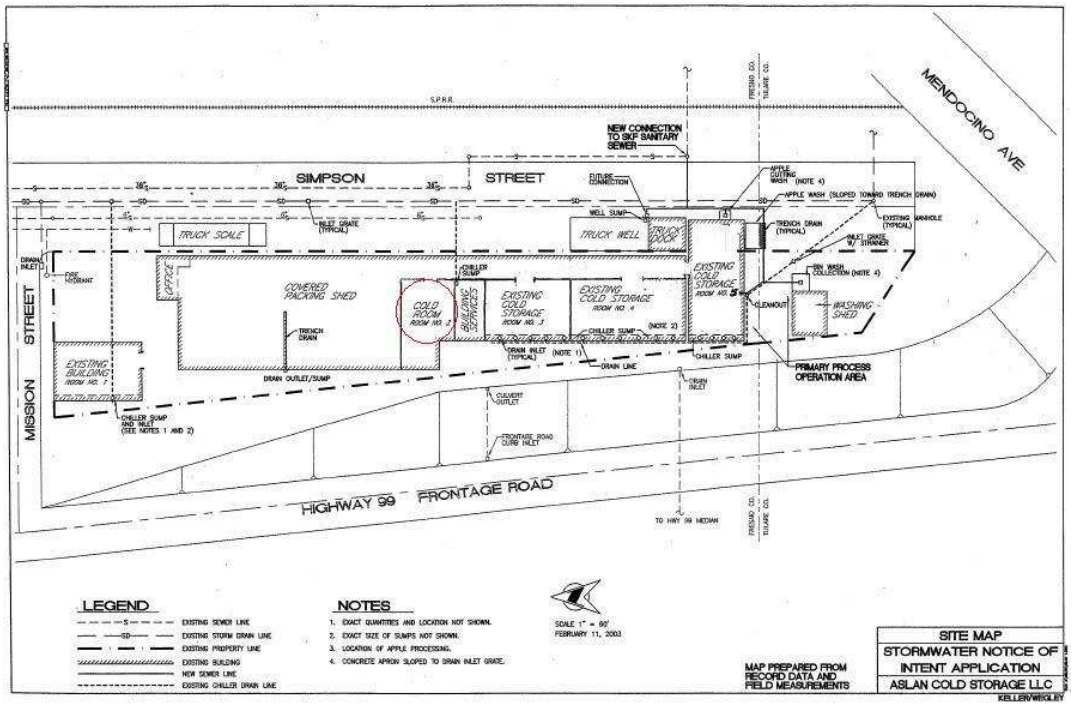

Figure 4.2: Room location at the facility.

surface area of the coils is kept between -4 and 0^oC $(24.8 - 32^oF)$. Due to the humidity inside the room, a defrost cycle is triggered by a timer every 12 hours. Ammonia is compressed by five compressors of different capacities, which are used for all the rooms in the facility. The power consumption of the compressors consists of two $45kW$ $(60hp)$ units, two $93kW$ $(125hp)$ units and one $298kW$ $(400hp)$ unit. It is not possible to directly measure the exact amount of compressor power utilized for a specific room. Heat is dissipated by the cooling towers at the back of the facility. An expansion valve controls the flow of ammonia refrigerant to the coils closing the refrigerant cycle.

In order to obtain data of regular operating conditions in the warehouse and the liquid desiccant system, a number of sensors were installed in Room 2. The sensors are connected to the data acquisition system (see Fig. 4.3) which logs at a sample rate of one minute and allows remote access of the data. A list of the sensors and equipment installed is described below:

1. Obvius DAQ Model AcquiSuite A8812. DA Server Serial number AA10F3 (see Figure 4.3).

2. Temperature sensor Veris TW Series. Serial Number: 22676 22675. Range: 0^oC to 50^oC (output signal 4 to 20mA). Measurement: Room temperature. Two locations in the room. With accuracy of $\pm 0.3^oC$.

3. Current monitoring Veris Model: Hawkeye 300 (H300). Range: 0.15 to 60A. Measurement: Ammonia valve status.

4. Humidity and temperature transmitter Vaisala. Serial number C2940001. Range: -40^oC to 60^oC (output signal 0 to 10V), 0 to 100 % RH (output signal 0 to 10V). Measurement: Inlet air RH and T. With accuracy of $\pm 0.2^oC$ in temperature and $\pm 1.0\%$ RH (0 to $90\%RH$) or $\pm 1.7\%RH$ (90 to $100\%RH$).

5. Temperature and Humidity sensor Veris. Model: T Series RTD/Thermistor. Serial number: Z201652−OH. Measurement: Ambient temperature and relative humidity. Accuracy of $\pm 0.3^oC$.

6. Temperature sensor Veris Model: AA10. Range: -29^oC to 69^oC (output signal 4 to 20mA). Measurement: Coil surface temperature. Two locations. Accuracy of $\pm 0.3^oC$.

7. Differential Pressure transducer SETRA Model 264. Range: 0 to 0.25 in.w.c (4 to 20 mA) P/N 2641R25WDIITIC. Measurement: Air pressure drop.

8. Flow meter Omega Model FP-5300 Serial number: 60706220447. Range: 0 to 200 gpm (output signal: frequency value). Measurement: Water flow rate. Accuracy of $\pm 0.5\%$.

9. Temperature sensor Veris. Model: AA10. Range: 0^oC to 100^oC (output signal 4 to 20mA). Measurement: Inlet water temperature. Accuracy of $\pm 0.3^oC$.

10. Digital RTD. Range: -18.05^oC to 537.5^oC (output signal 0 to 10V). Resistor 3K ohm. Measurement: Outlet water temperature. Accuracy of $\pm 0.3^oC$.

11. Frequency/Pulse signal conditioner Omega. Output range: 4 to 20 mA. Measurement: Signal conditioner for flow meter Signal conditioner.

Figure 4.4 shows the location of the sensors as well as some components of the refrigeration cycle. The sensors have been mounted at different locations within the facility and the operating range of each one has been determined by considering the operating conditions and location within the system.

Each sensor was connected to an AcquiSuite data acquisition system that has available space for eight analog channels, and the capability of adding multiple expansion units that provide four analog and four pulse channels each. Data are collected at a rate of one minute, under specific names for each of the variables being measured, and stored in a server at Bridgeover, Inc. These data can be accessed remotely by using the proprietary software r-Meter that checks for a pre-assigned password for each user. The software allows the user to view measured values over a desired length of time. Figure 4.5 shows a screen shot of the tool used to view the collected data.

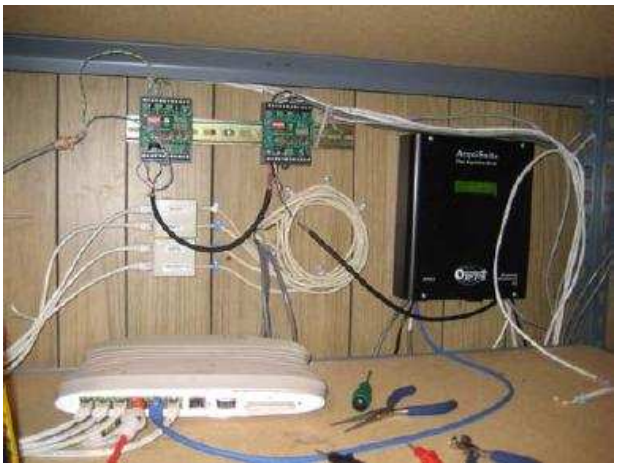

Figure 4.3: Data acquisition system and transmitter.

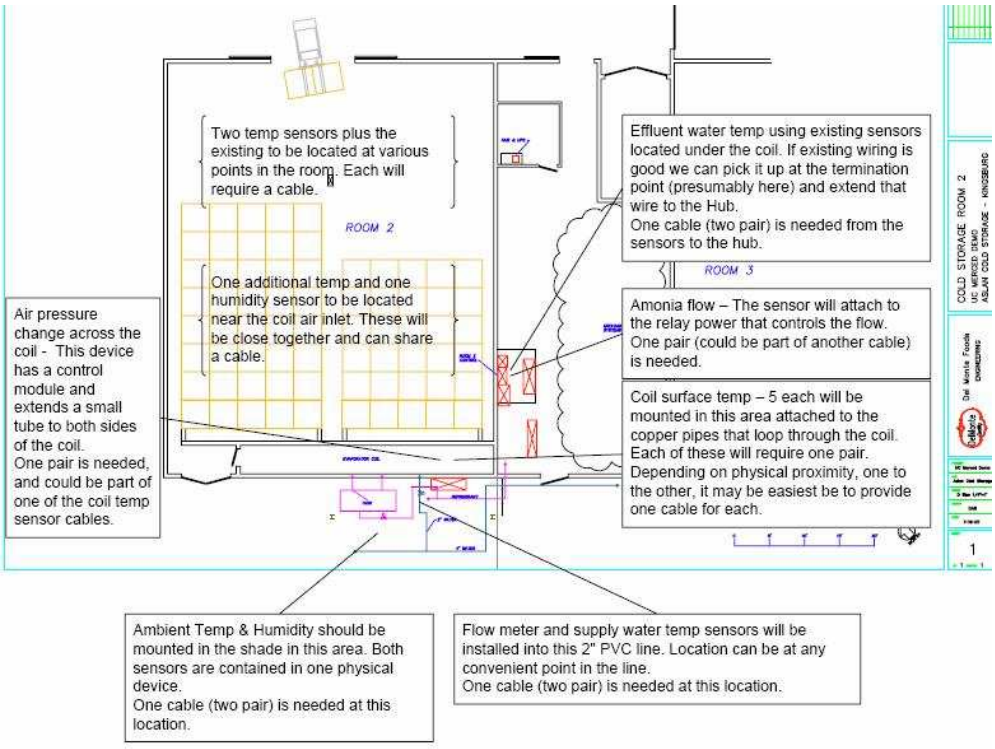

Figure 4.4: Schematic showing the location of sensors.

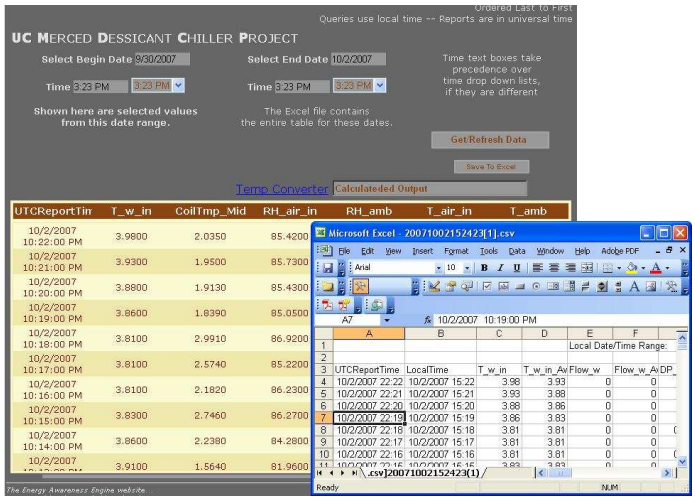

Figure 4.5: Example of collected data.

4.2 Components and integration of the liquid desiccant system

This subsection describes the components of the system including off-the-shelf items such as pumps, fans, filters, FPGA, and a tank, as well as several sensors that are used to monitor the performance of the system. It also describes the assembly of the liquid desiccant system and the integration with the selected warehouse at Kingsburg.

4.2.1 Components of the liquid desiccant system

The following corresponds to the list of components that were acquired for the integration of the liquid desiccant system.

1. Absorber: Manufactured by AIL Research. Case modeled: 100 plates, 0.4 m^3/s (833 cfm), 1.1^oC (34^oF) dry-bulb and 0^oC (32^oF) dew point. The final dimensions are in Fig. 4.6.

2. Regenerators: Manufactured by AIL Research. Case modeled: 100 plates, 0.4 m^3/s (833 cfm), 1.1^oC (34^oF) dry-bulb and 0^oC (32^oF) dew point. (see Fig. 4.7).

3. Internal heat exchanger (IHX). From AIL Research (see Fig. 4.8).

4. Exhaust Fan, Medium Duty Direct Drive, Propeller diameter 0.51 m (20 In), 1.62 m^3/s (3440 cfm), Model: 4YC98 (Grainger).

5. Liquid-cooled mini magnetic drive centrifugal pump, 5.0 gpm, 115 VAC, Model: EG-07142-02 (Cole-Palmer).

6. Float type flow meters (rotameters) 1/2 in PVC fitting, Model: 4350K41 (McMaster Carr).

7. Two 20 microns water filter with clear styrene housing and 3/4 in NPT female connections, 10 gpm flow, Model: 4422K3 (McMaster Carr).

8. Magnetic drive centrifugal pump with PP-coated magnet, 10 gpm, 115 VAC, Model: K-07022-21 (Cole-Palmer).

9. Exhaust Fan, Medium Duty Direct Drive, Propeller diameter 24 In, 4435 cfm, Model: 4C363 (Grainger).

10. Compact SBC for 44 pin PIC with Ethernet, RS232 interface and TCP/IP stack, Revision 2 board, Model: SBC65EC. Fully assembled with PIC18F452 CPU and 24LC256 EEPROM included with IOR5E Input-Output-Relay board with an enclosure and a battery backed RTC (Modtronix).

11. Speed Control, Rotary, Adjustable, Voltage 115, Max Amps 6, Max Wattage 720, Plate Color Silver, Height 4 1/2 In, Width 2 3/4 In, Depth 1 1/2 in, Model: 1DGV2 (Grainger).

12. 300 Gallon high-density-polyethylene with UV inhibitors vertical-closed-head Tank (US Plastics Corp).

13. Two HO series Temperature/Relative humidity, 3 %, $4-20mA$, -40 to 50 ^oC, $0-100$ % sensors (Veris). This is used for air conditions downstream of the absorber. With accuracy of $\pm 0.3^oC$ in temperature and $\pm 5\%$ RH.

14. HD Series Relative humidity sensor for ambient air conditions, 3 %, $4-20mA$, Model: HD3XMSX (Veris). With accuracy of $\pm 5\%$.

15. 264 $XMIT$ differential pressure transducer with 25 $i.w.c.$ range. (Setra). Used to measure liquid desiccant level inside tank.

16. Four TC Series temperature sensors $4-20mA$, -50 to 50 ^oC (Veris). Located downstream of Absorber.With accuracy of $\pm 0.3^oC$.

17. Three TI Series temperature sensors $4-20mA$, -50 to 50 ^oC (Veris). Used to measure inlet liquid desiccant temperature to internal heat exchanger, inlet liquid desiccant temperature to absorber, and outlet liquid desiccant temperature from Absorber. Accuracy of $\pm 0.3^oC$.

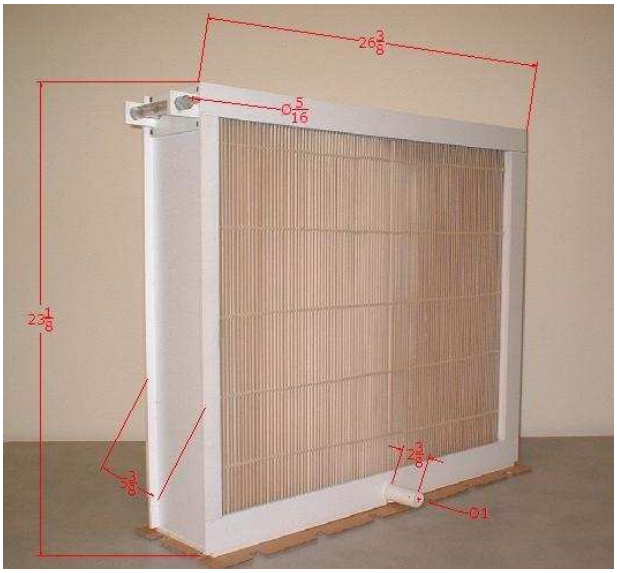

Figure 4.6: Absorber by AIL Research. 100 plates, $0.4 m^3/s$ (833 cfm), 1.1^oC (34^oF) dry-bulb and 0^oC (32^oF) dew point. Figure shows the dimensions in British units because of design.

18. Air - Water Flow Sensor With 0 to 5 Vdc Output, model FLR1011, $0.1 - 2$ SLM (Omega). Accuracy of $\pm 1\%$.

19. Penn Plax air Pod Silent Aquarium Air Pump - 20 Gallons. Used to measure liquid desiccant level inside tank.

20. 300 gallons of calcium chloride 37 % percent concentration Tech grade. Purchased from Univar.

Figure 4.7: Regenerators by AIL Research. 100 plates, $0.4m^3/s$ (833 cfm), 1.1^oC (34^oF) dry-bulb and 0^oC (32^oF) dew point.

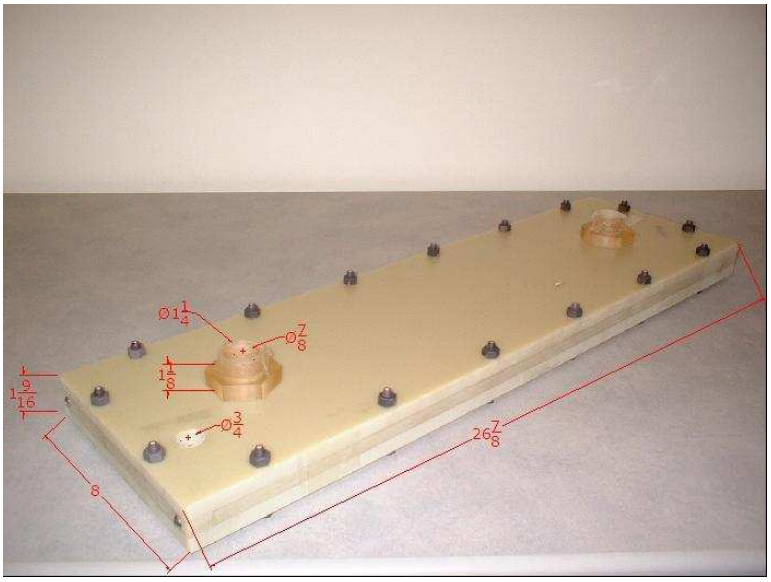

Figure 4.8: Internal heat exchanger IHX. Figure shows the dimensions in British units because of design.

4.2.2 Integration of the liquid desiccant system

A preliminary design of the final assembly was developed after receiving all the components and checking their manufactured dimensions. The main issues of the design were the support to withstand the vibrations from fans, and the static load from heat/mass exchangers and internal heat exchanger. The stands needed to acomodate the installation of the sensors and devices as well as wiring, piping and hoses.

Stands, design and construction

The geometric design was made considering the device dimensions as well as optimum use of available materials. The final design is shown in Fig. 4.9
The materials were selected based on the operating conditions of the system. Treated wood was selected for the absorber/IHX stand because of the humidity and temperature conditions inside the cold storage. Traditional wood was selected for the regenerators stands. Galvanized brackets and screws were used to join the wood and to provide stability to the structure. Figure 4.10 shows the basic structures (with fans) before the installation of the devices.

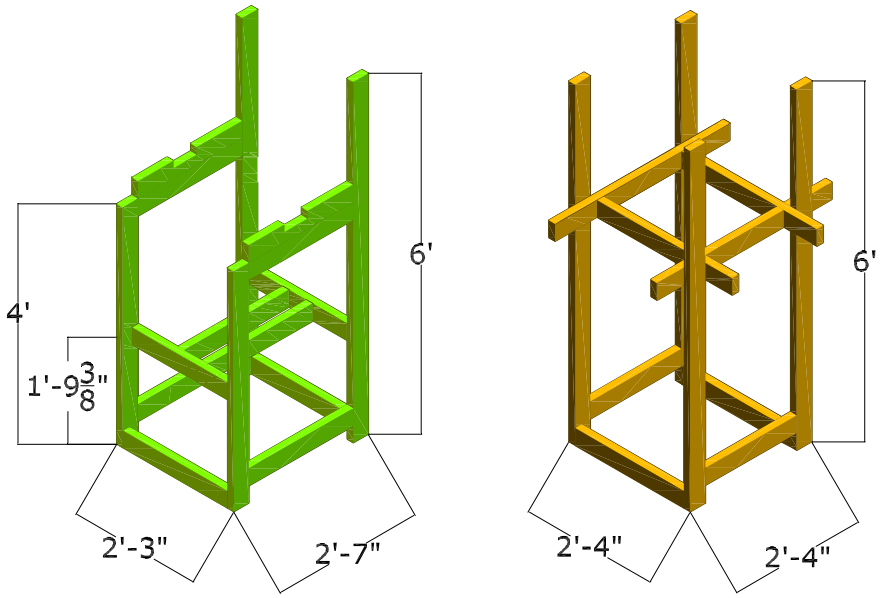

Figure 4.9: Stand Design. *a*) Absorber, *b*) Regenerators. Figure shows the dimensions in British units because of design.

Placing the stands and integration of the system

Figure 4.11 shows the location of the absorber, and regenerator stands as well as the location of the tank. The absorber was located in a secured area were no damage to the equipment could happen as a result of the normal operation of the cold storage.

Figure 4.10: Absorber/IHX and Regenerator stands

Figure 4.11: Final setup of the system

Chapter 5

Mathematical model of the Absorber

5.1 Energy balance approach

An adiabatic dehumidifier heat and mass exchanger with a zigzag longitudinal −plate configuration is initially modeled beginning with an energy balance. Although an energy balance applied to the absorption process does not include the influence of the geometry, it constitutes a first approximation that provides preliminary understanding of the absorber's performance.

Since the amount of water absorbed is small compared to the mass flow rate of liquid desiccant, the thickness of the film is assumed constant. No active cooling

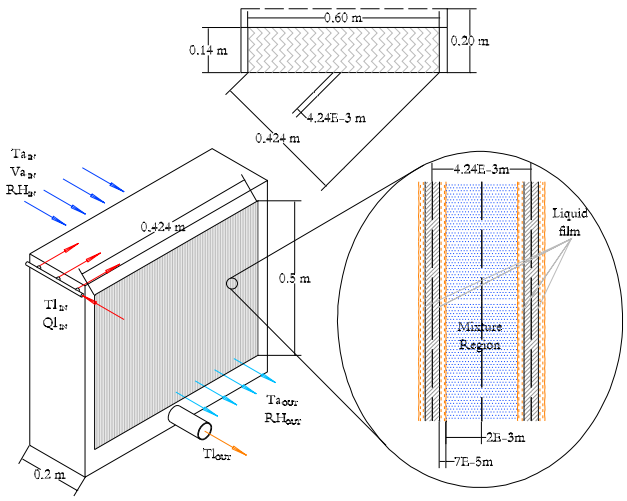

Figure 5.1: Dimensions for the absorber device

is used to remove heat from the walls of the absorber so the model considers an adiabatic core. The purpose of this dehumidifier is to extract humidity from the air stream; consequently, the outlet temperature of the air stream is increased. The free flow area of the core is considered for the air side as shown in Fig. 5.1 The energy balance corresponds to:

$$\dot{m}_l Cp_l \Delta T_l = \dot{m}_a (Cp_a \Delta T_a - h_{gf} \Delta \omega), \tag{5.1}$$

where the mass flow rate for liquid desiccant and air are denoted by $\dot{m}_l$ and $\dot{m}_a$, respectively. ΔT_l and ΔT_a are the change in temperature between inlet and outlet conditions for the liquid and air streams, respectively, and the enthalpy of condensation is represented by h_{gf}. From this equation, it is possible to obtain the

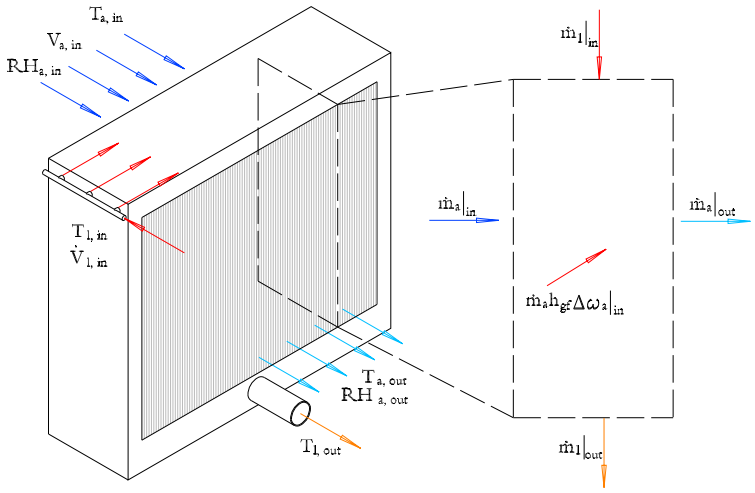

Figure 5.2: Schematic of adiabatic dehumidifier showing mass and species balances

change in humidity ratio $\Delta\omega$. The elements for this energy balance are depicted in Fig. 5.2.

5.2 Two dimensional constant thickness approximation

A more detailed model was developed by discretizing the liquid desiccant and air-subdomains. A parallel flow model and a counter flow model with constant thickness were analyzed. Those two dimensional numerical approximations were compared against the benchmark works from [25, 28, 34].

Considering laminar flow and fully developed conditions for the liquid desiccant film and the air, the falling liquid moves in the positive x_l direction (film direction) and the air goes in the same direction for the parallel flow case, and from the bottom to the top in the counter flow case (film direction). The thicknesses for both, liquid film and air were kept fixed as it is shows in the Fig. 5.3. Velocity in the transverse $y_{l,a}$ direction is considered negligible. The flow of the liquid desiccant is considered smooth so that no wavy motion was modeled. Physical properties were considered constant. Thermodynamic equilibrium was assumed at the interface. The momentum inlet conditions were considered as parabolic profiles with nonslip condition at the wall for the liquid film and maximum velocity for the air at the axis of symmetry. Air was considered as ideal gas, body forces were not considered and no shear forces were exerted by the air on the film. Initial and boundary conditions for the condensation phenomena are shown in the energy and mass balance where diffusion in $x_{l,a}$ directions is negligible, the rate of water vapor absorption is small and the solubility of air in the desiccant is negligible.

5.2.1 Momentum balance in the film

From assumptions given before and the general expression for momentum balance

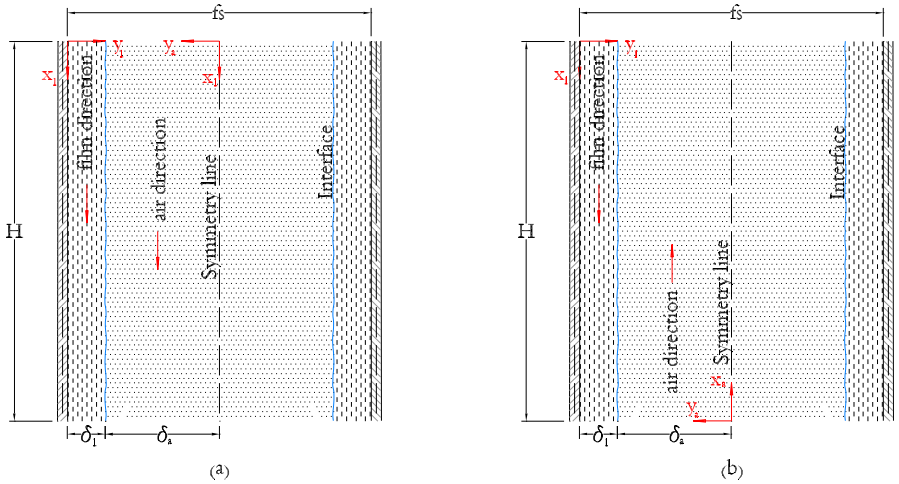

Figure 5.3: Schematic diagram of vertical channel between falling film and air (a) parallel flow (b) counter flow

$$\rho\frac{DV}{Dt} = -\nabla p - [\nabla\tau] + \rho g, \tag{5.2}$$

the equation of motion takes the form

$$\mu_l\frac{\partial^2 u_l}{\partial y_l^2} + \rho_l g = 0, \tag{5.3}$$

with boundary conditions

$$y_l = 0;\ u_l = 0, \tag{5.4}$$

$$y_l = \delta_l;\ \frac{\partial u_l}{\partial y_l} = 0. \tag{5.5}$$

Integrating twice with respect to y_l, the analytical expression for velocity takes the form

$$u_l = \frac{g}{\nu_l}\left(\delta_l y_l - \frac{y_l^2}{2}\right). \tag{5.6}$$

Now, from continuity across the film and considering L=1m for the width of the wall, the expression for film thickness in the film as function of the mass flow rate and velocity profile becomes

$$\dot{m}_l = \int_0^{\delta_l} \rho_l u_l dy_l, \tag{5.7}$$

$$\delta_l = \left(\frac{3\dot{m_l}\nu_l}{\rho_l g}\right)^{\frac{1}{3}}, \tag{5.8}$$

$$u_l = \frac{3}{2}u_{l,me}\left[2\left(\frac{y_l}{\delta_l}\right) - \left(\frac{y_l}{\delta_l}\right)^2\right], \tag{5.9}$$

where $u_{l,me}$ is the mean velocity as is expresed below

$$u_{l,me} = \frac{\dot{m}_l}{\rho_l \delta_l}. \tag{5.10}$$

5.2.2 Energy and mass balance in the film

Considering the assumptions given above and from the general expression for energy balance

$$\rho \hat{C}p\frac{DT}{Dt} = k\nabla^2 T + \mu\Phi_v, \tag{5.11}$$

the energy balance takes the form

$$\rho \hat{Cp}_l u_l \frac{\partial T_l}{\partial x_l} = k_l \frac{\partial^2 T_l}{\partial y_l^2}, \tag{5.12}$$

with boundary conditions

$$x_l = 0;\ T_l = T_{l,i}, \tag{5.13}$$

$$y_l = 0;\ T_l = T_w,\ or,\ y_l = 0;\ \frac{\partial T_l}{\partial y_l} = 0, \tag{5.14}$$

$$y_l = \delta_l;\ T_l = T_a. \tag{5.15}$$

The boundary condition in Eq. (5.14) depends if we are computing for the benchmark or for the actual problem respectively.

The mass balance equation can be obtained in a similar way. Then the balance takes the form

$$u_l \frac{\partial C}{\partial x_l} = D_l \frac{\partial^2 C}{\partial y_l^2}. \tag{5.16}$$

with boundary conditions

$$x_l = 0;\ C = C_i \tag{5.17}$$

$$y_l = 0;\ \frac{\partial C}{\partial y_l} = 0. \tag{5.18}$$

5.2.3 Momentum balance in the air

For the air region it is possible to apply a momentum balance as was done in the liquid part. Neglecting gravity effects on the air, the momentum equation is as follows

$$\frac{\partial p}{\partial x} = \mu_a \frac{\partial^2 u_a}{\partial y_a^2}, \tag{5.19}$$

with boundary conditions

$$y_a = 0;\ \frac{\partial u_a}{\partial y_a} = 0, \tag{5.20}$$

$$y_a = \delta_a;\ u_a = u_l. \tag{5.21}$$

Using momentum and continuity equations it is possible to get also an analytical expression for velocity air profile as a function of pressure gradient in x_a direction, δ_l, δ_a and y as it is shown bellow

$$u_a = u_{l,int} - \frac{dp}{dx}\frac{1}{2\mu_a}(\delta_a^2 - y_a^2), \tag{5.22}$$

where

$$\frac{dp}{dx} = \frac{3u_{l,int}\mu_a}{\delta_a^2} - \frac{3\mu_a \dot{m}_a}{2\rho_a \delta_a^3 L}, \tag{5.23}$$

thus

$$u_a = u_{l,int}\left[\frac{3}{2}(\frac{y_a}{\delta_a})^2 - \frac{1}{2}\right] + \frac{3}{4}\frac{\dot{m}_a}{\rho_a \delta_a^3 L}(\delta_a^2 - y_a^2), \tag{5.24}$$

where $u_{l,int}$ is consider positive for parallel flow and negative for counter flow.

In function of mean air velocities, the profile is expresed as

$$u_a = \frac{3}{2}u_{l,me}\left[\frac{3}{2}(\frac{y_a}{\delta_a})^2 - \frac{1}{2}\right] + \frac{3}{4}u_{a,me}\left[1 - (\frac{y_a}{\delta_a})^2\right], \tag{5.25}$$

where $u_{a,me}$ is

$$u_{a,me} = \frac{\dot{m}_a}{\rho_a \delta_a L}. \tag{5.26}$$

5.2.4 Energy and mass balance in the air

As in the liquid region, the derivation for energy and mass balance are represented by

$$u_a \frac{\partial T_a}{\partial x_a} = \alpha_a \frac{\partial^2 T_a}{\partial y_a^2}, \tag{5.27}$$

$$u_a \frac{\partial W}{\partial x_a} = D_a \frac{\partial^2 W}{\partial y_a^2}, \tag{5.28}$$

with boundary conditions

$$x_a = 0;\ T_a = T_{a,i};\ W = W_i, \tag{5.29}$$

$$y_a = 0;\ \frac{\partial T_a}{\partial y_a} = 0;\ \frac{\partial W}{\partial y_a} = 0, \tag{5.30}$$

$$y_a = \delta_a;\ T_l = T_a;\ W = W_{int}. \tag{5.31}$$

where W_{int} and p_v are

$$W_{int} = 0.62185\frac{p_v}{(p_t - p_v)}, \tag{5.32}$$

$$p_v = p_{v,H_2O}\left[1 - 0.828Cc - 1.496Cc^2 + Cc\frac{(T_{int} - 40)}{350}\right], \tag{5.33}$$

$$p_{v,H_2O} = 610.78exp\left[\frac{17.269T_{int}}{(237.3 + T_{int})}\right]. \tag{5.34}$$

5.2.5 Interface energy and species balances

At $y_l = \delta_l$ and $0 \leqslant x \leqslant H$ the interface liquid-air has its own balance as it is shown in the Fig. 5.4

$$-k_l\frac{\partial T_l}{\partial y_l} = k_a\frac{\partial T_a}{\partial y_a} + \rho_a D_a h_{fg}\frac{\partial W}{\partial y_a}, \tag{5.35}$$

$$-\rho_l D_l\frac{\partial C}{\partial y_l} = \rho_a D_a\frac{\partial W}{\partial y_a}. \tag{5.36}$$

5.2.6 Dimensional analysis

Nondimensional variables are taken from [35, 36] and introduced as follows

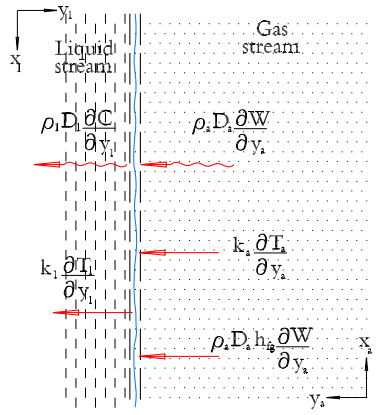

Figure 5.4: Schematic interface balance

$$X_l = \frac{4}{Pe_l}\frac{x_l}{\delta_l},\ X_a = \frac{4}{Pe_a}\frac{x_a}{(\frac{fs}{2}-\delta_l)}, \tag{5.37}$$

$$Y_l = \frac{y_l}{\delta_l},\ Y_a = \frac{y_a}{(\frac{fs}{2}-\delta_l)}, \tag{5.38}$$

$$U_l = \frac{u_l}{u_{l,me}},\ U_a = \frac{u_a}{u_{a,me}}, \tag{5.39}$$

$$\Theta_l = \frac{T_l}{T_{l,i}},\ \Theta_a = \frac{T_a}{T_{a,i}}, \tag{5.40}$$

$$\Lambda_l = \frac{C}{C_i},\ \Lambda_a = \frac{W}{W_i}, \tag{5.41}$$

$$Pe_l = Pr_l Re_l,\ Pr_l = \frac{\nu_l}{\alpha_l},\ Re_l = \frac{4u_{l,me}\delta_l}{\nu_l}, \tag{5.42}$$

$$Pe_{m,l} = Sc_l Re_l,\ Sc_l = \frac{\nu_l}{D_l}, \tag{5.43}$$

$$Pe_a = Pr_a Re_a,\ Pr_a = \frac{\nu_a}{\alpha_a},\ Re_a = \frac{4u_{a,me}(\frac{fs}{2}-\delta_l)}{\nu_a}, \tag{5.44}$$

$$Pe_{m,a} = Sc_a Re_a,\ Sc_a = \frac{\nu_a}{D_a}, \tag{5.45}$$

$$Le_l = \frac{D_l}{\alpha_l},\ Le_a = \frac{D_a}{\alpha_a}, \tag{5.46}$$

where the heat transfer Peclet numbers for the liquid desiccant and the air are Pe_l and Pe_a, respectively, as well as the mass transfer peclect numbers $Pe_{m,l}$ and $Pe_{m,a}$.

With these dimensionless variables the velocity profiles for the air and the liquid desiccant take the form

$$U_l = \frac{3}{2}(2Y_l - Y_l^2), \tag{5.47}$$

$$U_a = \frac{3}{4}((3\Pi_1 - 1)Y_a^2 - \Pi_1 + 1), \tag{5.48}$$

where the non dimensional coefficient Π_1 is

$$\Pi_1 = \frac{u_{l,me}}{u_{a,me}}. \tag{5.49}$$

After applying the transformations, the governing equations for the heat and mass transfer in the liquid film and air regions become

$$U_{l,a}\frac{\partial \Theta_{l,a}}{\partial X_{l,a}} = \frac{\partial^2 \Theta_{l,a}}{\partial Y_{l,a}^2}, \tag{5.50}$$

$$U_{l,a}\frac{\partial \Lambda_{l,a}}{\partial X_{l,a}} = Le_{l,a}\frac{\partial^2 \Lambda_{l,a}}{\partial Y_{l,a}^2}. \tag{5.51}$$

with the following boundary conditions

$$X_{l,a} = 0;\ 0 \leqslant Y_{l,a} \leqslant 1;\ \Theta_{l,a} = 1;\ \Lambda_{l,a} = 1, \tag{5.52}$$

$$Y_{l,a} = 0;\ 0 \leqslant X_{l,a} \leqslant 1;\ \frac{\partial \Theta_{l,a}}{\partial Y_{l,a}} = 0;\ \frac{\partial \Lambda_{l,a}}{\partial Y_{l,a}} = 0, \tag{5.53}$$

$$Y_{l,a} = 1;\ 0 \leqslant X_{l,a} \leqslant 1;\ \Theta_l = \frac{T_{a,i}}{T_{l,i}}\Theta_a;\ \Lambda_a = \frac{W_{int}}{W_i}. \tag{5.54}$$

Similarly, for the interface energy and species balance

$$-\Pi_A \frac{\partial \Theta_l}{\partial Y_l} = \frac{\partial \Theta_a}{\partial Y_a} + \Pi_B \frac{\partial \Lambda_a}{\partial Y_a}, \tag{5.55}$$

$$-\Pi_C \frac{\partial \Lambda_l}{\partial Y_l} = \frac{\partial \Lambda_a}{\partial Y_a}, \tag{5.56}$$

where the non dimensional coefficients Π_A, Π_B and Π_C are

$$\Pi_A = \frac{k_l T_{l,i}(fs/2 - \delta_l)}{k_a T_{a,i} \delta_l}, \tag{5.57}$$

$$\Pi_B = \frac{\rho_a D_a h_{gf} W_i}{k_a T_{a,i}}, \tag{5.58}$$

$$\Pi_C = \frac{\rho_l D_l C_i (fs/2 - \delta_l)}{\rho_a D_a W_i \delta_l}. \tag{5.59}$$

5.2.7 Two dimensional numerical approximation

Equations (5.12, 5.16, 5.27, 5.28) or equations (5.50 and 5.51) need to be discretized. Governing equations of energy and mass transfer for both air and liquid falling film are solved using finite difference approximation. The

axial convection terms are approximated by upstream differences and the diffusion terms are expressed by central differences. The following procedure was adapted from Ali and Vafai [37] and will be employed in the analysis:

(a) Input inlet conditions for mass flow rate, temperature, humidity ratio, and concentration for both air and desiccant film as well as and the dimension of the device.

(b) Calculate the film thickness and pressure gradient from the custom formulas and then compute the velocity profiles for the air and liquid desiccant film.

(c) Assume interfacial humidity ratio and temperature for the whole domain ($y_l = \delta_l$ or $y_a = \delta_a$, $0 \leq x \leq H$.

(d) Solve the humidity ratio for the air and desiccant concentration by marching through the whole domain.

(e) Solve the temperature distribution for the desiccant film and air by marching through the whole domain.

(f) Compute the interfacial air concentration from Eq. (5.32). for the whole domain. Now it is possible to find a new interfacial temperature and concentration at the liquid side.

(g) If the maximum error between the calculated values and assumed ones are greater than the convergence criterion, update the assumed interface values by the calculated values and repeat $(d)-(g)$ until the values of the interfacial humidity ratio converges.

Benchmark for two dimensional numerical approximation

A comparison with the work done by Rahamah [34] for parallel flow, and Ali [28] for parallel and counter flow validated the 2D numerical model developed which is tested for the list of parameters values presented in Table 5.1 and Figs. 5.5 and 5.6.

Figure 5.5 (a) shows that variations in air humidity ratio do not affect the average profiles of air and desiccant temperature. Conversely, Fig. 5.5 (b) indicates that as inlet air humidity ratio increases the rate of dehumidification increases too. Water concentration in the liquid desiccant and in air are calculated keeping constant inlet air and liquid desiccant temperature and constant water concentration in the liquid region as well. Figure 5.6 shows a counter flow example under similar operating conditions as in parallel flow example. The average air temperature decreases from the inlet value approaching the liquid desiccant temperature as shown in Fig. 5.6 (a). As the air is dehumidified, the water concentration in the liquid increases towards the outlet as depicted in Fig. 5.6 (b).

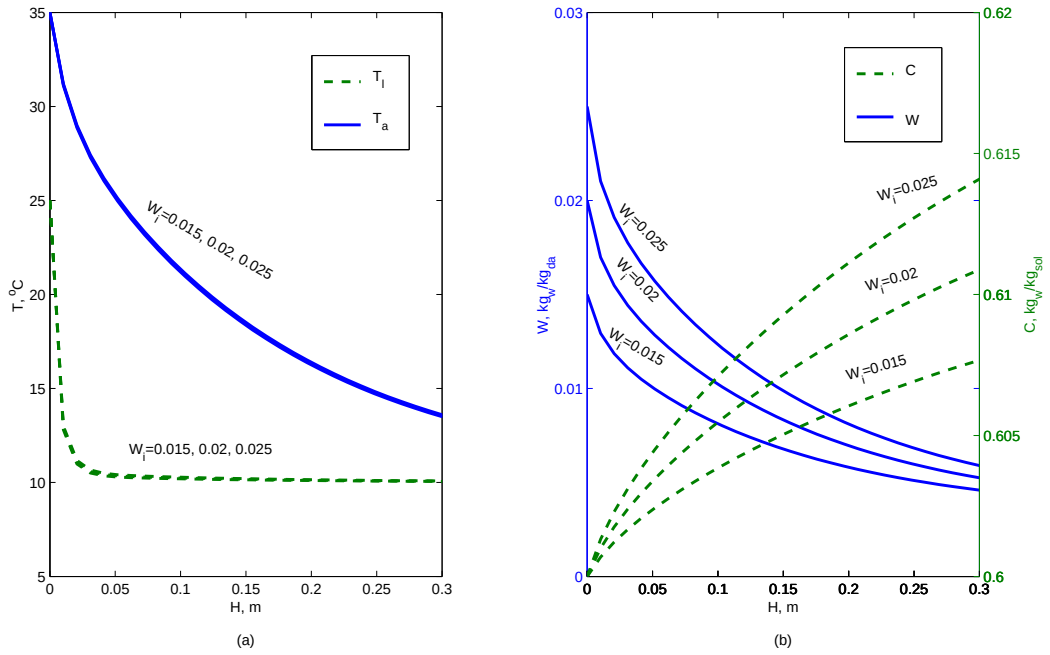

Figure 5.5: Variation of W, C, T_a and T_l along the wall for different values of W_i at $T_{a,i} = 30^oC$, $C_i = 0.6$, $T_{d,i} = 25^oC$ in parallel flow

The average Nusselt number Nu_{avg} and average Sherwood number Sh_{avg} based on the inlet air temperature and inlet humidity ratio are determined from

$$Nu_{avg} = \frac{d_h}{H}\int_0^H \left[\frac{(\partial T_a/\partial y_a)_{y_a=\delta_a}}{(T_{a,i} - T_{int})}\right] dx, \tag{5.60}$$

$$Sh_{avg} = \frac{d_h}{H}\int_0^H \left[\frac{(\partial W/\partial y_a)_{y_a=\delta_a}}{(W_i - W_{int})}\right] dx, \tag{5.61}$$

where the hydraulic diameter is defined as $d_h = 4(\frac{fs}{2} - \delta_l)$.

A comparison of the results obtained with the model developed in this study and the works by [34] and Ali [28] is shown in Table 5.2, where Nu_{avg} and Sh_{avg}

Table 5.1: Operating parameters and properties used in the first comparison

Parameter	Units	Desiccant region	Air region
$T_{a,i}$	^oC		35
$T_{l,i}$	^oC	21	
W_i	$kg_w kg_{da}^{-1}$		0.02
C_i	$kg_w kg_{sol}^{-1}$	0.6	
$\dot{m}_a$	kgs^{-1}		0.0125
$\dot{m}_l$	$kgm^{-1}s^{-1}$	0.007	
T_{wall}	^oC	10	
k	$Wm^{-1}K^{-1}$	0.525	0.02635
Cp	$Jkg^{-1}K^{-1}$	2330	1028
ρ	kgm^{-3}	1394	1.172
μ	$kgm^{-1}s^{-1}$	1.19×10^{-2}	1.83×10^{-5}
D	m^2s^{-1}	4.2×10^{-10}	2.5×10^{-5}
h_{fg}	Jkg^{-1}		2.448×10^6

where using Eqs. (5.60) and (5.61) respectively. Properties and inlet conditions were taken from Ali [28] and Mesquita [25]. This is the reason why the errors from Rahamah are greater than Ali's.

Table 5.2: Comparison between Nusselt and Sherwood numbers for the actual investigation, Rahamah and Ali

		Rahamah		Actual Inv.		% error	
H	L	Nu_{avg}	Sh_{avg}	Nu_{avg}	Sh_{avg}	Nu_{avg}	Sh_{avg}
0.4	0.0033	2.93	2.50	3.15	2.81	6.98	11.03
0.5	0.0033	2.45	2.07	2.65	2.34	7.55	11.54
0.6	0.0033	2.08	1.75	2.27	2.00	8.37	12.50
0.7	0.0033	1.84	1.51	1.98	1.74	7.07	13.22
0.4	0.0030	2.68	2.25	2.90	2.58	7.59	12.79
0.4	0.0035	3.08	2.67	3.30	2.96	6.66	9.79
0.4	0.0040	3.44	2.95	3.65	3.30	5.75	10.61
		Ali Inv.		Actual Inv.		% error	
H	L	Nu_{avg}	Sh_{avg}	Nu_{avg}	Sh_{avg}	Nu_{avg}	Sh_{avg}
0.4	0.0033	3.04	2.73	3.15	2.81	3.50	2.85
0.5	0.0033	2.54	2.25	2.65	2.34	4.15	3.85
0.6	0.0033	2.18	1.91	2.27	2.00	3.96	4.50
0.7	0.0033	1.89	1.65	1.98	1.74	4.55	5.17
0.4	0.0030	2.79	2.49	2.90	2.58	3.79	3.49
0.4	0.0035	3.19	2.88	3.30	2.96	3.33	2.70
0.4	0.0040	3.55	3.24	3.65	3.30	2.74	1.81

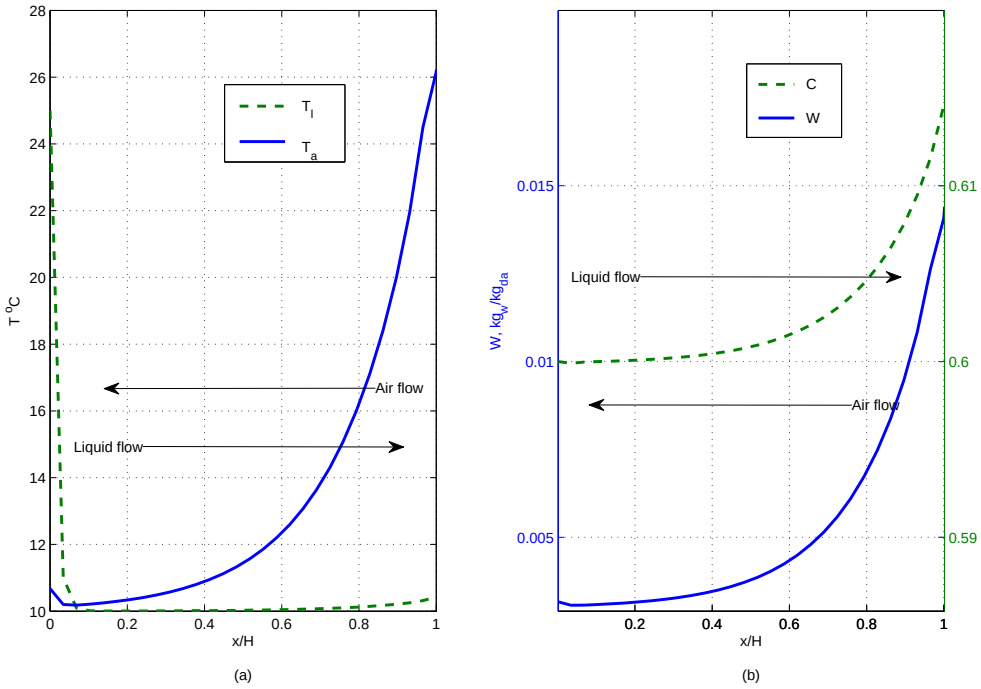

Figure 5.6: Variation of W, C, T_a and T_l along the wall for $W_i = 0.015$ at $T_{a,i} = 27^oC$, $C_i = 0.6$, $T_{d,i} = 25^oC$ in counter flow

5.3 Three dimensional approximation

A cross flow model between a falling liquid desiccant film and a horizontal air stream is studied in three dimensions, as depicted in Fig. 5.7. The model is adapted from the works by Park [38, 39, 40, 41] and Ali [37].

Considering a laminar, fully developed flow for the liquid desiccant film and the air, the falling liquid falls down in the positive y direction and the air moves in the positive x direction. The rate of water vapor absorption is small and the solubility of air in the desiccant is negligible so the film thickness is considered constant. The velocity of the liquid desiccant in the z_l direction is zero. The flow is assumed to be smooth, implying no wavy motion exists. The physical properties are considered constant and thermodynamic equilibrium is assumed at the interface. The liquid desiccant velocity inlet condition is taken as a parabolic profile with the no−slip condition at the wall and zero gradient at the interface with the air. For the air, a no−slip condition was assumed at the interface and a maximum velocity was expected at the symmetry plane. Air is modeled as an ideal gas, body forces were only identified for the liquid desiccant and no shear forces were exerted by the air on the film.

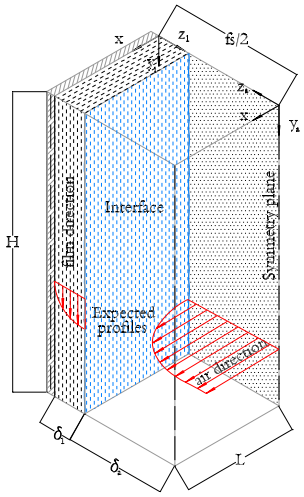

Figure 5.7: Schematic of cross flow falling film absorber

5.3.1 Mass and momentum balance in the film

We consider the velocity of the liquid desiccant in the z_l and x directions to be zero. From continuity, the variation of the velocity of the film in the y direction is also zero.

$$\frac{\partial v}{\partial y} = 0. \tag{5.62}$$

The general expression for the momentum balance is

$$\rho \frac{D\vec{V}}{Dt} = -\nabla p - [\nabla \tau] + \rho g. \tag{5.63}$$

Applying the assumptions stated previously the equation of motion simplifies to

$$\mu_l \frac{\partial^2 v}{\partial z_l^2} + \rho_l g = 0, \tag{5.64}$$

with boundary conditions

$$z_l = 0;\ 0 \leqslant y \leqslant H;\ 0 \leqslant x \leqslant L;\ v = 0, \tag{5.65}$$

$$z_l = \delta_l;\ 0 \leqslant y \leqslant H;\ 0 \leqslant x \leqslant L;\ \frac{\partial v}{\partial z_l} = 0. \tag{5.66}$$

Integrating twice with respect to z_l, we obtain an analytical expression for velocity

$$v(z_l) = \frac{g}{\nu_l}\left(\delta_l z_l - \frac{z_l^2}{2}\right). \tag{5.67}$$

From continuity across the film and considering constant properties in the x direction, an expression for the film thickness as function of the mass flow rate is obtained as follows

$$\delta_l = \left(\frac{3\dot{m_l}\nu_l}{\rho_l g}\right)^{\frac{1}{3}}. \tag{5.68}$$

Similar expressions are presented by Mills and Incropera [6, 42].

5.3.2 Energy and species balance in the film

The energy balance is simplified to

$$v\frac{\partial T_l}{\partial y} = \alpha_l \frac{\partial^2 T_l}{\partial z_l^2}, \tag{5.69}$$

with boundary conditions

$$y = 0;\ 0 \leqslant z_l \leqslant \delta_l;\ 0 \leqslant x \leqslant L;\ T_l = T_{l,i}, \tag{5.70}$$

$$z_l = 0;\ 0 \leqslant y \leqslant H;\ 0 \leqslant x \leqslant L;\ \frac{\partial T_l}{\partial z_l} = 0, \tag{5.71}$$

$$z_l = \delta_l;\ 0 \leqslant y \leqslant H;\ 0 \leqslant x \leqslant L;\ T_l = T_a. \tag{5.72}$$

The species equation takes the form

$$v\frac{\partial C}{\partial y} = D_l \frac{\partial^2 C}{\partial z_l^2}. \tag{5.73}$$

with boundary conditions

$$y = 0;\ 0 \leqslant z_l \leqslant \delta_l;\ 0 \leqslant x \leqslant L;\ C = C_i, \tag{5.74}$$

$$z_l = 0;\ 0 \leqslant y \leqslant H;\ 0 \leqslant x \leqslant L;\ \frac{\partial C}{\partial z_l} = 0. \tag{5.75}$$

5.3.3 Mass and momentum balance in moist air

Similar to the liquid part, the velocity of the air in the x and y directions are considered negligible, and the continuity equation is simplified to

$$\frac{\partial u}{\partial x} = 0. \tag{5.76}$$

In this case, the $x-$momentum equation is required

$$\frac{\partial p_a}{\partial x} = \mu_a \frac{\partial^2 u}{\partial z_a^2}, \tag{5.77}$$

with boundary conditions

$$z_a = 0;\ 0 \leqslant y \leqslant H;\ 0 \leqslant x \leqslant L;\ \frac{\partial u}{\partial z_a} = 0, \tag{5.78}$$

$$z_a = \delta_a;\ 0 \leqslant y \leqslant H;\ 0 \leqslant x \leqslant L;\ u = 0. \tag{5.79}$$

Using momentum and continuity equations, an analytical expression for the u velocity profile is obtained as follows

$$u = \frac{1}{2\mu_a} \frac{\partial p}{\partial x} \left(z_a^2 - \delta_a^2 \right), \tag{5.80}$$

where

$$\frac{\partial p_a}{\partial x} = -\frac{3\mu_a \dot{m}_a}{\rho_a \delta_a^3 H}, \tag{5.81}$$

as presented by Mills [6] and Incropera [42].

5.3.4 Energy and species balance in moist air

The energy and species balance are represented by the next expressions

$$u\frac{\partial T_a}{\partial x} = \alpha_a \frac{\partial^2 T_a}{\partial z_a^2}, \tag{5.82}$$

$$u\frac{\partial W}{\partial x} = D_a \frac{\partial^2 W}{\partial z_a^2}, \tag{5.83}$$

with boundary conditions

$$x = 0;\ 0 \leqslant y \leqslant H;\ 0 \leqslant z_a \leqslant \delta_a;\ T_a = T_{a,i};\ W = W_i, \tag{5.84}$$

$$z_a = \delta_a;\ 0 \leqslant y \leqslant H;\ 0 \leqslant x \leqslant L;\ T_l = T_a;\ W = W_{int}, \tag{5.85}$$

$$z_a = 0;\ 0 \leqslant y \leqslant H;\ 0 \leqslant x \leqslant L;\ \frac{\partial T_a}{\partial z_a} = 0;\ \frac{\partial W}{\partial z_a} = 0, \tag{5.86}$$

where W_{int} and p_v are calculated from equations (5.32), (5.33) and (5.34). Vapor pressure (p_v) is formulated in terms of vapor pressure of water at the same temperature (p_{v,H_2O}), and the relative vapor pressure (π),

$$p_v = p_{v,H_2O}\pi, \tag{5.87}$$

the calcium chloride concentration (Cc), and temperature at the interface (T_{int}). Expression for (π) is taken from Ali [37] but can also be obtained using Conde's work [43, 44]. Also, several properties of moist air are computed using Singh [45].

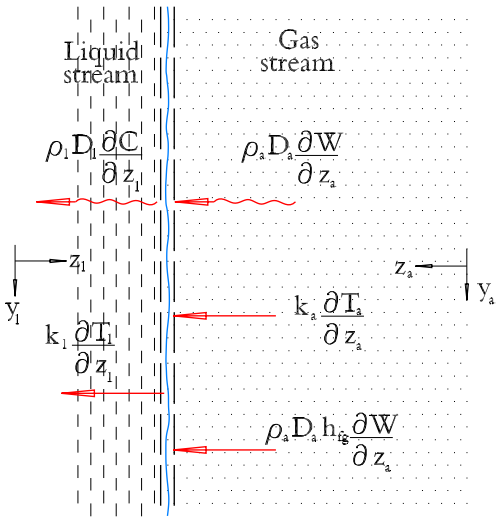

Figure 5.8: Interface energy and species balances

5.3.5 Interface energy and species balances

At $z_l = \delta_l$, $0 \leqslant x \leqslant L$ and $0 \leqslant y \leqslant H$ the liquid−air interface balance is shown in Fig. 5.8.

$$-k_l \frac{\partial T_l}{\partial z_l} = k_a \frac{\partial T_a}{\partial z_a} + \rho_a D_a h_{gf} \frac{\partial W}{\partial z_a}, \tag{5.88}$$

$$-\rho_l D_l \frac{\partial C}{\partial z_l} = \rho_a D_a \frac{\partial W}{\partial z_a}. \tag{5.89}$$

Continuity of temperature at the interface is applied but the concentration is in general discontinuous. Also, the interface concentration is obtained from Eq. (5.32), once the interface temperature is known. Assuming thermodynamic equilibrium at the interface and the air mixture to be an ideal gas, the vapor pressure

of the liquid desiccant ($p_{v,l}$) at the interface is equal to the partial pressure of the water vapor ($p_{v,a}$) in the air-vapor mixture.

$$z_l = \delta_l;\ z_a = \delta_a;\ 0 \leqslant y \leqslant H;\ 0 \leqslant x \leqslant L;\ T_l = T_a;\ p_{v,l} = p_{v,a}. \tag{5.90}$$

5.3.6 Dimensional analysis

Nondimensional variables are taken from [41, 35, 36] and introduced as follows

$$X_l = \frac{x}{L};\ X_a = \frac{4}{Pe_a}\frac{x}{(\frac{fs}{2} - \delta_l)}, \tag{5.91}$$

$$Y_l = \frac{4}{Pe_l}\frac{y}{\delta_l};\ Y_a = \frac{y}{H}, \tag{5.92}$$

$$Z_l = \frac{z_l}{\delta_l},\ Z_a = \frac{z_a}{(\frac{fs}{2} - \delta_l)}, \tag{5.93}$$

$$V = \frac{v}{v_{me}},\ U = \frac{u}{u_{me}}, \tag{5.94}$$

$$\Theta_l = \frac{T_l}{T_{l,i}},\ \Theta_a = \frac{T_a}{T_{a,i}}, \tag{5.95}$$

$$\Lambda_l = \frac{C}{C_i},\ \Lambda_a = \frac{W}{W_i}, \tag{5.96}$$

$$Pe_l = Pr_l Re_l,\ Pr_l = \frac{\nu_l}{\alpha_l},\ Re_l = \frac{4 v_{me}\delta_l}{\nu_l}, \tag{5.97}$$

$$Pe_{m,l} = Sc_l Re_l,\ Sc_l = \frac{\nu_l}{D_l}, \tag{5.98}$$

$$Pe_a = Pr_a Re_a,\ Pr_a = \frac{\nu_a}{\alpha_a},\ Re_a = \frac{4 u_{me}(\frac{fs}{2} - \delta_l)}{\nu_a}, \tag{5.99}$$

$$Pe_{m,a} = Sc_a Re_a,\ Sc_a = \frac{\nu_a}{D_a}, \tag{5.100}$$

$$Le_l = \frac{D_l}{\alpha_l},\ Le_a = \frac{D_a}{\alpha_a}, \tag{5.101}$$

where the heat transfer Peclet numbers for the liquid desiccant and the air are Pe_l and Pe_a respectively, as well as the mass transfer peclect numbers $Pe_{m,l}$ and $Pe_{m,a}$.

With the dimensionless variables the velocity profiles for the air and the liquid desiccant take the form

$$V = \frac{3}{2}(2Z_l - Z_l^2), \tag{5.102}$$

$$U = \frac{3}{2}(1 - Z_a^2). \tag{5.103}$$

After applying the transformations, the governing equations for the heat and mass transfer in the liquid film become

$$V\frac{\partial \Theta_l}{\partial Y_l} = \frac{\partial^2 \Theta_l}{\partial Z_l^2}, \tag{5.104}$$

$$V\frac{\partial \Lambda_l}{\partial Y_l} = Le_l\frac{\partial^2 \Lambda_l}{\partial Z_l^2}, \tag{5.105}$$

with boundary conditions as follows

$$Y_l = 0;\ 0 \leqslant Z_l \leqslant 1;\ 0 \leqslant X_l \leqslant 1;\ \Theta_l = 1;\ \Lambda_l = 1, \tag{5.106}$$

$$Z_l = 0;\ 0 \leqslant Y_l \leqslant \frac{4}{Pe_l}\frac{H}{\delta_l};\ 0 \leqslant X_l \leqslant 1;\ \frac{\partial \Theta_l}{\partial Z_l} = 0;\ \frac{\partial \Lambda l}{\partial Z_l} = 0, \tag{5.107}$$

$$Z_l = \delta_l;\ 0 \leqslant Y_l \leqslant \frac{4}{Pe_l}\frac{H}{\delta_l};\ 0 \leqslant X_l \leqslant 1;\ \Theta_l = \frac{T_{a,i}}{T_{l.i}}\Theta_a. \tag{5.108}$$

Similarly, for the heat and mass transfer in the air, the governing equations become

$$U\frac{\partial \Theta_a}{\partial X_a} = \frac{\partial^2 \Theta_a}{\partial Z_a^2}, \tag{5.109}$$

$$U\frac{\partial \Lambda_a}{\partial X_a} = Le_a\frac{\partial^2 \Lambda_a}{\partial Z_a^2}, \tag{5.110}$$

with the following boundary conditions

$$X_a = 0;\ 0 \leqslant Y_a \leqslant 1;\ 0 \leqslant Z_a \leqslant 1;\ \Theta_a = 1;\ \Lambda_L = 1, \tag{5.111}$$

$$Z_a = 1;\ 0 \leqslant Y_a \leqslant 1;\ 0 \leqslant X_a \leqslant \frac{4}{Pe_a}\frac{L}{(\frac{fs}{2} - \delta_l};\ \Theta_a = \frac{T_{l,i}}{T_{a,i}}\Theta_l, \tag{5.112}$$

$$Z_a = 0;\ 0 \leqslant Y_a \leqslant 1;\ 0 \leqslant X_a \leqslant \frac{4}{Pe_a}\frac{L}{(\frac{fs}{2} - \delta_l};\ \frac{\partial \Theta_a}{\partial Z_a} = 0;\ \frac{\partial \Lambda_a}{\partial Z_a} = 0. \tag{5.113}$$

Similarly, for the interface energy and species balance

$$-\Pi_A\frac{\partial \Theta_l}{\partial Z_l} = \frac{\partial \Theta_a}{\partial Z_a} + \Pi_B\frac{\partial \Lambda_a}{\partial Z_a}, \tag{5.114}$$

$$-\Pi_C\frac{\partial \Lambda_l}{\partial Z_l} = \frac{\partial \Lambda_a}{\partial Z_a}. \tag{5.115}$$

The average Nusselt number Nu_{avg} and average Sherwood number Sh_{avg} based on the inlet air temperature and inlet humidity ratio are determined from

$$Nu_{avg} = \frac{d_h}{H}\int_0^H \int_0^L \left[\frac{(\partial T_a/\partial z_a)_{z_a=(fs/2-\delta_a)}}{(T_{a,i}-T_{int})}\right] dxdy, \tag{5.116}$$

$$Sh_{avg} = \frac{d_h}{H}\int_0^H \int_0^L \left[\frac{(\partial W/\partial z_a)_{z_a=(fs/2-\delta_a)}}{(W_i-W_{int})}\right] dxdy, \tag{5.117}$$

where the hydraulic diameter is defined as $d_h = 4(\frac{fs}{2} - \delta_l)$.

5.3.7 Three dimensional numerical approximation

Equations (5.69, 5.73, 5.82, 5.83) or equations (5.104, 5.105, 5.109, 5.110) need to be discretized. Governing equations of energy and mass transfer for both air and liquid falling film were solved using a finite difference approximation [46, 47]. The axial convection terms are approximated by upstream differences and the diffusion terms are expressed by central differences. Figure 5.9 shows a schematic of the nodes location within the domains. The procedure described in the Section 5.2.7 is followed assuming interfacial humidity ratio and temperature for the whole domain ($z_l = \delta_l$ or $z_a = \delta_a$, $0 \leq x \leq L$ and $0 \leq y_{a,l} \leq H$) in item (c).

The model was validated against the results obtained by Park [38] for ambient temperature conditions. Table 5.3 shows the results of the comparison where

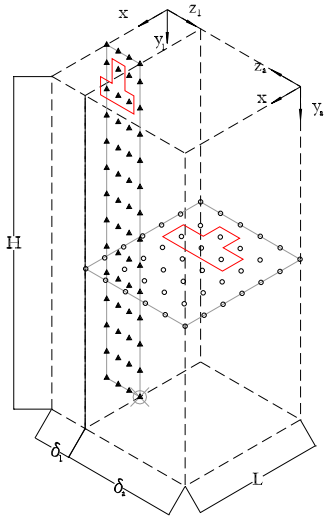

Figure 5.9: 3D discretization scheme

Table 5.3: Comparison between outlet air temperature and humidity ratio for the actual investigation and Park

				Park		Current		
Cc_{in} (%)	$T_{l,in}$ (^oC)	W_{in}	$T_{a,i}$ (^oC)	W_{out}	$T_{a,out}$ (^oC)	W_{out}	$T_{a,out}$ (^oC)	error (%)
75	23.28	20.89	29.44	11	22.1	10.9	23.6	6.9
76	23.67	21.03	29.56	11	22.5	10.9	24	6.7
78	24.00	20.95	29.51	12	23.4	11.8	24.3	4
80	24.00	20.82	29.61	11	23.5	10	24.3	3.5
82	24.72	21.09	29.61	10	23.6	9.8	25	6

the percentage errors were computed using the outlet temperatures. Uncertainty in the values of the fluid properties and the grid size account for most of the discrepancies. However the results show that the model can be used to predict the behavior of a cross-flow heat and mass exchanger using liquid desiccants.

Chapter 6

Results and discussion

6.1 Sensitivity analysis of the experimental data

Quantification of the absorption process is obtained from the inlet and outlet data collected from the absorber at the Aslan Cold Storage facility $(T, RH, \dot{m})$. Using temperature and relative humidity, upstream and downstream of the core, the change in air humidity ratio is found, and consequently the absorption rate is calculated. The results depend on the spatial location of the sensors as well as their accuracy. The location of the sensors is subject to the space and operational constrains of the industrial facility.

Under low temperature conditions, the content of water vapor in air is low even at the maximum relative humidity. Thus, it is necessary to evaluate the impact

of the sensors accuracy on humidity ratio. Relative humidity and temperature measurements at the inlet point of the core as well as the outlet conditions were taken with a HO Veris sensor which has an accuracy of $\pm 0.3^{o}C$ in temperature and $\pm 3\%$ RH. From a selected set of data where the operative conditions of the warehouse were stable, the confidence intervals from 90% to 75% were obtained as shows Fig. 6.1.

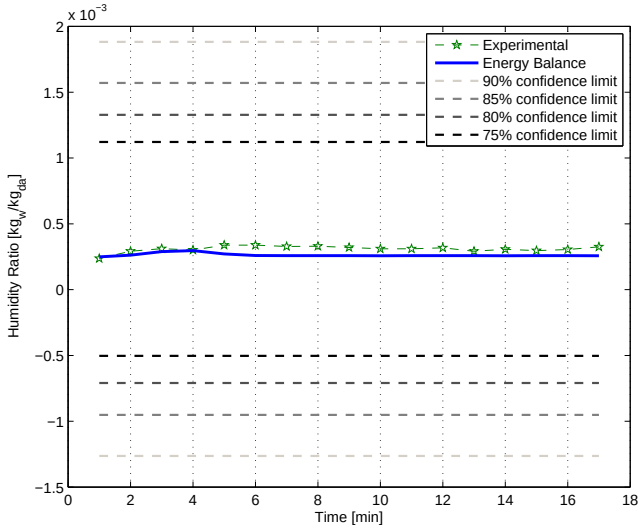

Figure 6.1: Confidence intervals for a selected set of data under relatively stable inlet conditions.

6.2 Experimental results

The change in the absorption capacity is directly related to the conditions of relative humidity and temperature at the entrance of the absorber and the liquid

desiccant concentration. As was expected, for low values of relative humidity and low temperature, the rate of water absorption was less than for large values of both relative humidity and temperature at a relatively constant liquid desiccant concentration and mass flow rates of air and liquid desiccant.

The energy balance model developed in section 5.1 was initially verified with a graphic comparison between experimental absorption data that can be obtained by the difference between the inlet and outlet humidity ratio. The results are sufficiently close in spite of the precision of the sensors. Changes in temperature affect the results of the energy balance more than changes in relative humidity.

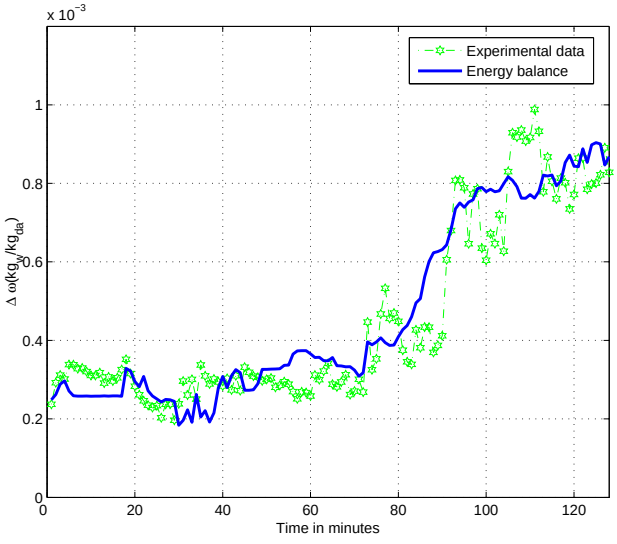

Figure 6.2: Variation of the experimental and predicted humidity ratio with respect to time

Figure 6.2 shows the change in humidity ratio with respect to time obtained from the test data and with the energy balance. The values were computed from the inlet and outlet measurement of T and RH at the absorber. The figure also shows the values of $\Delta\omega$ obtained using the energy balance described by Eq. (5.1).
An additional source of uncertainty is the uneven wetting of the core walls with liquid desiccant. Average differences of 0.27^oC in temperature and 3.2% in RH were found across the core's surface when the liquid desiccant was not able to be spread uniformly.

6.3 Numerical results

A comparative numerical approximation of a heat and mass transfer for an adiabatic parallel-plate absorber for which a thin film of liquid desiccant flows down its walls and dehumidifies the air in cross-flow configuration was developed. The performance of the absorber is analyzed as a function of inlet air temperature and relative humidity, inlet liquid desiccant temperature, mass flow rates of air and liquid desiccant, and liquid desiccant concentration.
Table 6.1 shows the properties used to run the simulation for the cold storage conditions. Contours of interfacial and average film and air properties (temperature and concentration) were obtained for specific operating conditions. Figure

Table 6.1: Operating parameters and properties used

Parameter	Units	Desiccant region	Air region
$T_{a,i}$	^oC		$0-5$
$T_{l,i}$	^oC	$5-8$	
W_i	$kg_w kg_{da}^{-1}$		$0.006-0.002$
C_i	$kg_w kg_{sol}^{-1}$	0.65	
$\dot{m}_a$	kgs^{-1}		0.00328
$\dot{m}_l$	$kgm^{-1}s^{-1}$	0.001786	
k	$Wm^{-1}K^{-1}$	0.525	0.02635
Cp	$Jkg^{-1}K^{-1}$	2330	1028
ρ	kgm^{-3}	1394	1.172
μ	$kgm^{-1}s^{-1}$	1.19×10^{-2}	1.83×10^{-5}
D	m^2s^{-1}	4.2×10^{-10}	2.5×10^{-5}
h_{fg}	$Jkg^{-1}K^{-1}$		2.448×10^6

6.3 shows the distribution of water concentration in the liquid desiccant at the interface. The portion of the liquid desiccant flowing near the entrance of the air side shows larger levels of water content compared to section near the end of the absorber's depth.

This driving potential for mass transfer also affects the temperature distribution at the interface, as shown in Fig. 6.4. Since air enters the absorber at a low temperature, the rise in liquid desiccant temperature due to condensation is not significant. Figure 6.5 shows the moist distribution on the air side at the interface between air and liquid desiccant in cross flow configuration. The strongest desorption occurs at the air and liquid entrance affecting the profiles mainly in those regions.

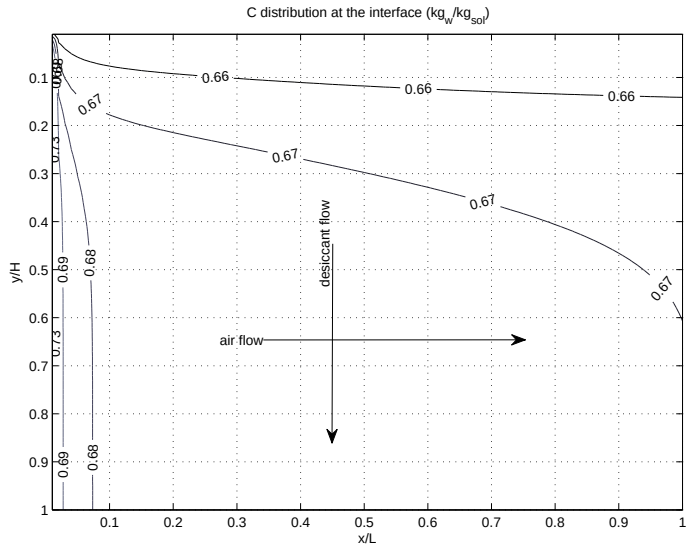

Figure 6.3: Distribution of water concentration at the interface in the liquid domain.

Average distribution of water concentration in the full air and liquid domains are presented in Figs. 6.6 and 6.7. The concentration is seen to decrease in its flow direction but to increase in the air flow direction, for the liquid and air-side, respectively.

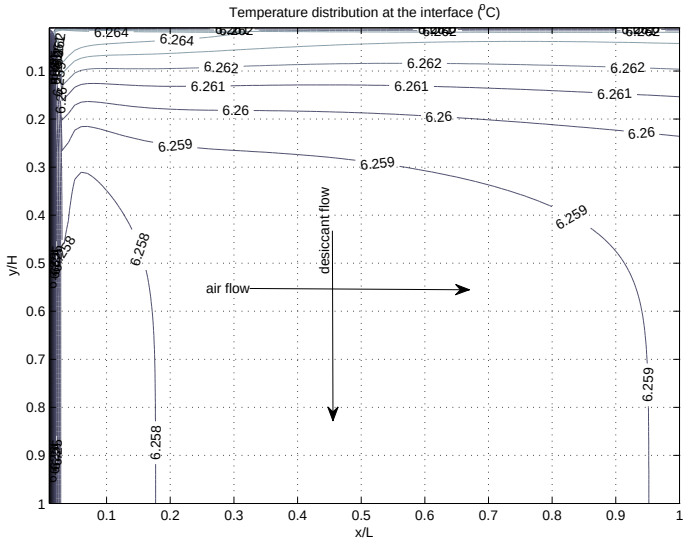

Figure 6.4: Distribution of Temperature at the interface for both air and liquid domain.

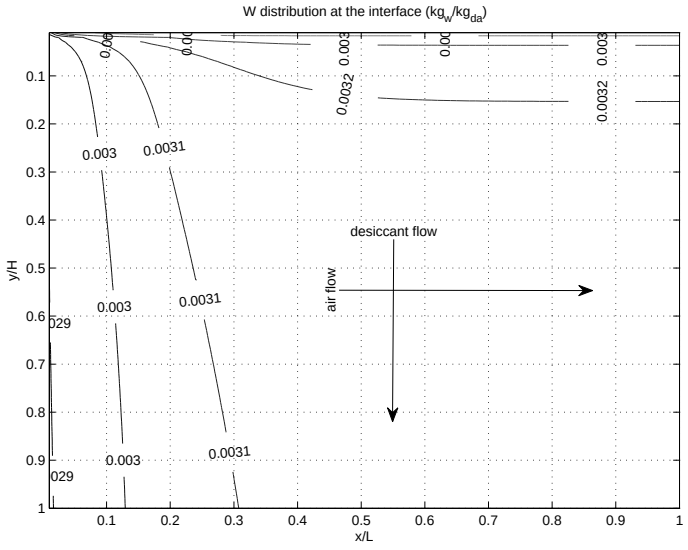

Figure 6.5: Distribution of water concentration at the interface in the air domain.

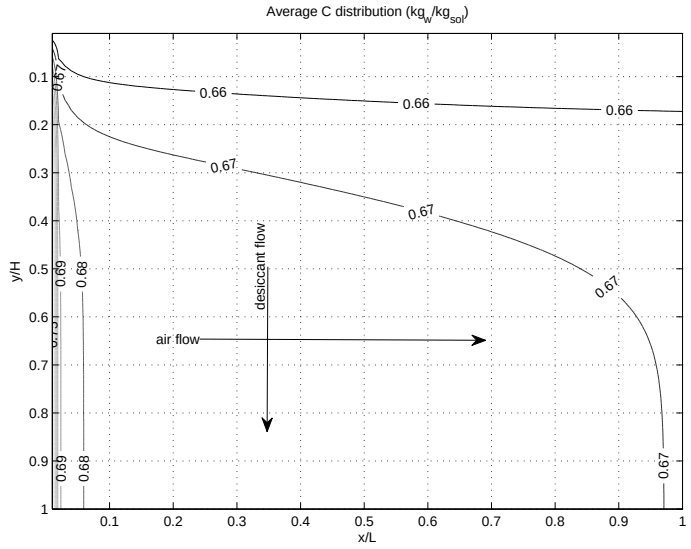

Figure 6.6: Average distribution of water concentration in the liquid domain.

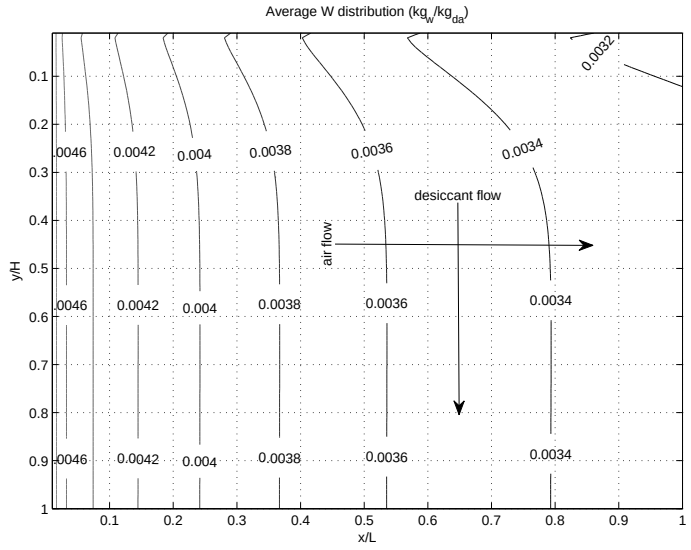

Figure 6.7: Average distribution of water concentration in the air domain.

6.3.1 Application of model to industrial site conditions

The purpose of the liquid desiccant system is to remove the moisture of the air before it reaches the surface of the evaporator where it would condensate forming a layer of ice, thus preventing the air flow in the evaporator and isolating it in the process of heat absorption. If the absorber lowers the dew point temperature of the air to a value below the surface temperature of the evaporator coil, condensation will not occur.

Consequently, test data of realistic operating conditions inside a cold storage were obtained from the facilities at Aslan Cold Storage. Temperature and relative humidity measurements were obtained for the air upstream of the evaporator as well as for the liquid desiccant at the absorber's outlet. Also, temperature at the evaporator's surface was collected. The numerical model of the absorber developed in this work was used to design a dehumidifier core that would remove moisture of the air avoiding the formation of frost on the evaporator's surface. Figure 6.8 depicts the values of the dew point temperature of the air upstream of the evaporator together with the inlet air temperature and coil's surface temperature during a complete defrosting cycle. The figure also shows the predicted dew point temperature of the air exiting the heat and mass exchanger (HME), calculated using the numerical model and from the actual absorber.

Even though, the state of the art of the numerical model does not allow to match the experimental and predicted models as it does not consider the zigzag geometry of the absorber and the transient effects, it is shown that both predicted and HME's outlet dew point temperature of the air leaving the absorber are most of the time below the evaporator surface temperature preventing the formation of ice.

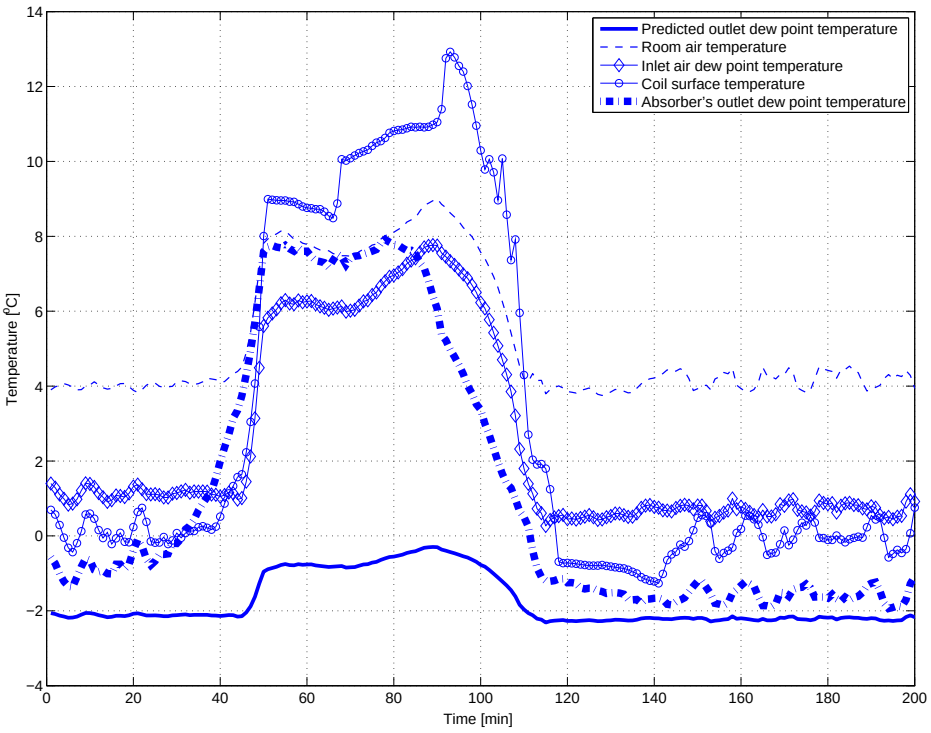

Figure 6.8: Comparison between inlet air dew point, a predicted outlet dew point from the numerical model and experimental absorber's outlet dew point temperatures.

Chapter 7

Conclusions and Recommendations

The coupled heat and mass transfer between a calcium chloride solution liquid desiccant falling film and moist air in cross flow was studied. Due to the low temperature of the air, an adiabatic absorber is utilized. Realistic operating conditions were obtained from a cold storage facility. The results show that an absorber can be designed to effectively eliminate the formation of ice on the surface of the evaporator.

The falling film absorbs moist from the room by vapor pressure difference between the liquid desiccant and the inlet air at low temperatures (0 to 15^oC). Moreover, the absorption process heats up the liquid desiccant but at the same time the air

cools it down allowing the assumption of constant properties properties all along the film. Nevertheless, by observation of the data down stream of the absorber it is possible to say that distribution of the liquid is not uniform.

Regular calculations were done using relative humidity and temperature at the inlet and the outlet of the absorber, looking for reference values of absorption (humidity ratio difference) for the predictive models developed. Range of uncertainties were obtained for each type of sensor used at those locations. The influence of the location and distribution of the sensors around the absorber, as well as, their precision, is considerable for the calculations. Furthermore, the inlet conditions for the absorber could be improved by the construction of an entrance tunnel that can hold a suitable set of sensors and at the same time homogenizes the air inlet. The actual conditions in the refrigerated warehouse facility used in this study do not allow its use.

Although the absorption is realized in small quantities (it is a low mass transfer process), the system is able to absorb a significant amount of water vapor in conditions of low temperature and low relative humidity. The predictive temperature of dew point shows that it can be kept below the temperature of the coil during the regular operation conditions, preventing ice formation on the coil surface and reducing water and energy consumption by avoiding defrosting cycles.

The geometric influence of the absorber's design was not studied, although it can cause a considerable increase in heat transfer by convection as well as the rate of absorption from the air to the liquid.

The liquid desiccant technology presented in this study is suitable for implementation in an industrial facility. However, strong precautions need to be taken in terms of using air and liquid desiccant filters to avoid changing the properties of the liquid desiccant due to contact with pollutants from dust, exhaust gases, etc. that are commonly found in industrial instalations. Also heat and mass exchanger damage implies liquid desiccant drop formation which can damage evaporator.

Bibliography

[1] Energy Information Administration. International energy outlook 2008 - highlights. Technical Report DOE/EIA-0484, Energy Information Administration, June 2008.

[2] International Energy Agency. World energy outlook 2006. Technical report, International Energy Agency, 2006.

[3] California Energy Commission Title 24 Buildings Energy Effuciency Standards. Refrigerated warehouses case report. Report, Pacific Gas and Electric Company, 2007.

[4] Pacific Gas and Electricity Company. Aggregated data for investor-owned utilities, publicly owned utilities, and combined utilities. appendix c. Technical report, California Energy Commission, 2007.

[5] Robert Byron Bird, Warren E. Steward, and Edwin N. Lightfoot. *Transport Phenomena*. John Wiley and Sons, second edition, 2002.

[6] Anthony F. Mills. *Basic heat and mass transfer*. IRWIN, 1995.

[7] Neil Petchers. *Combined heating, cooling and power handbook*. Fairmont Press, 2003.

[8] Y. K. Yadav. Vapour compression and liquid - desiccant hybrid solar space - conditioning system for energy conservation. *Renewable Energy*, 6(7):719–723, 1995.

[9] Feyka Scott and Vafai Kambiz. An investigation of a falling film desiccant dehumidification/regeneration cooling system. *Heat Transfer Engineering*, 28(2):163–172, 2007.

[10] Xiaohua Liu, Yi Jiang, Jianjun Xia, and Xiaomin Chang. Analytical solutions of coupled heat and mass transfer processes in liquid desiccant air dehumidifier/regenerator. *Energy Conservatins and Management*, 48:2221–2232, 2007.

[11] Cheng Qin Ren, Min Tu, and Hua Hui Wang. An analytical model for heat and mass transfer processes in internally cooled or heated liquid desiccantair contact units. *International Journal of Heat and Mass Transfer*, 50:3545–3555, 2007.

[12] K. Daou, R.Z. Wang, and Z.Z. Xia. Desiccant cooling air conditioning: a review. *Renewable and Sustainable Energy Reviews*, 10:55–77, 2006.

[13] Douglas R. Kosar. Dehumidification system enhancements. *ASHRAE Journal*, February 2006.

[14] Lewis G. Harriman III, Joseph Lstlburek, and Reinhold Kittler. Improving humidity control for commercial buildings. *ASHRAE Journal*, 42(11):24–32, November 2000.

[15] Sanjeev Jain and P.K. Bansal. Performance analysis of liquid desiccant dehumidification systems. *International Journal of Refrigeration*, 30:861–872, 2007.

[16] S. A. Abdul-Wahab, Y.H. Zurigat, and M.K. Abu-Arabi. Predictions of moisture removal rate and dehumidification effectiveness for structured liquid desiccant air dehumidifier. *Energy*, 29:19–34, 2004.

[17] Adnan A. Kinsara, Omar M. Rabghi, and Moustafa M. Elsayed. Parametric study of an energy efficient air conditioning system using liquid desiccant. *Applied Thermal Engineering*, 18(5):327–335, 1997.

[18] George O. G. Lof. *House Heating and Cooling with Solar Energy.* Madison: University of Wisconsin Press, 1995.

[19] Yonggao Yin and Xiaosong Zhang. A new method for determining coupled heat and mass transfer coefficients between air and liquid desiccant. *International Journal of Heat and Mass Transfer*, 51:3287–3297, 2008.

[20] Douglas R. Kosar, Michael J. Witte, Don B. Shirey III, and Roger L. Hedrick. Dehumidification issues of standard 62-1989. *ASHRAE Journal*, March 1998.

[21] Lewis G. Harriman III, Michael J. Witte, Marek Czachorski, and Douglas R. Kosar. Evaluating active desiccant systems for ventilating commercial buildings. *ASHRAE Journal*, October 1999.

[22] Thosapon Katejanekarn and S. Kumar. Performance of a solar-regenerated liquid desiccant ventilation pre-conditioning system. *Energy and Buildings*, 40:1252–1267, 2008.

[23] Sanjeev Jain, P.L. Dhar, and S.C. Kaushik. Experimental studies on the dehumidifier and regenerator of a liquid desiccant cooling system. *Applied Thermal Engineering*, 20:253–267, 2000.

[24] X.H. Liu, Y. Jiang, X.M. Chang, and X.Q. Yi. Experimental investigation of the heat and mass transfer between air and liquid desiccant in a cross-flow regenerator. *Renewal Energy*, 32:1623–1636, 2007.

[25] L.C.S. Mesquita, S.J. Harrison, and D. Thomey. Modeling of heat and mass transfer in parallel plate liquid-desiccant dehumidifiers. *Solar Energy*, 80:1475–1482, 2006.

[26] Arshad Y. Khan and Jorge L. Martinez. Modelling and parametric analysis of heat and mass transfer performance of a hybrid liquid desiccant absorber. *Energy Convers. Mgmt.*, 39(10):1095–1112, 1998.

[27] E. Mezaache and M. Daguenet. Effects of inlet conditions on film evaporation along an inclined plate. *Solar Energy*, 78:535–542, 2005.

[28] A. Ali, K. Vafai, and A.R.A. Khaled. Comparative study between parallel and counter flow configurations between air and falling film desiccant in the presence of nanoparticle suspensions. *International Journal of Energy Research*, 27:725–745, 2003.

[29] A. Ali and K. Vafai. An investigation of heat and mass transfer between air and desiccant film in an inclined parallel and counter flow channels. *International Journal of Heat and Mass Transfer*, 47:1745–1760, 2004.

[30] Lewis G. Harriman III and James Judge. Dehumidification equipment advances. *ASHRAE Journal*, 44(8):S22–S29, August 2002.

[31] ASHRAE. *Standards for Natural and Mechanical Ventilation*. ASHRAE, February 1973.

[32] S. Agunaga Bialous and S.A. Glantz. Ashrae standard 62: tobacco industry‘s influence over national ventilation standards. *Tobacco Control*, 11:315–328, September 2002.

[33] Andrew Persily. The revision of standard 62: What a difference a decade makes. In National Institute of stabdards and technology NIST, editors, *Preceedings: Indoor Air 2002, 9th International Cnference on Indoor Air Quality and Climate in Monterey, California*, pages 328–333. National Institute of stabdards and technology NIST, June 2002.

[34] A. Rahamah, M.M. Elsayed, and N.M. Al-Najem. A numerical solution for cooling and dehumidification of air by a falling desiccant film in parallel flow. *Renewable Energy*, 13(3):305–322, January 1998.

[35] G. Grossman. Simultaneous heat and mass transfer in film absorption under laminar flow. *Int. J. Heat Mass Transfer*, 26(3):357–371, 1983.

[36] G. Grossman and K. Gommed. Heat and mass transfer in film absorption in the presence of non-absorbable gases. *Int. J. Heat Mass Transfer*, 40(15):3595–3606, 1997.

[37] A. Ali, K. Vafai, and A.R.A. Khaled. Analysis of heat and mass transfer between air and falling film in a cross flow configuration. *International Journal of Heat and Mass Transfer*, 47:743–755, 2004.

[38] M. S. Park, John R. Howell, Gary C. Vliet, and John L. Peterson. Numerical and experimental results for coupled heat and mass transfer between a desiccant film and air in cross-flow. *International Journal of Heat and Mass Transfer*, 37:395–402, 1994.

[39] M. S. Park, John R. Howell, Gary C. Vliet, and John L. Peterson. Coupled heat and mass transfer between a falling desiccant film and air in cross flow: Part i - numerical model and experimental results. *AIAA/ASME Heat Transfer Conf. Colorado Springs*, 275:81–90, 1994.

[40] M. S. Park, Gary C. Vliet, and John R. Howell. Coupled heat and mass transfer between a falling desiccant film and air in cross flow: Part ii - parametric analysis and results. *AIAA/ASME Heat Transfer Conf. Colorado Springs*, 275:73–79, 1994.

[41] Moonsoo Park. *Analysis of couple heat and mass transfer between a falling desiccant film and air in cross flow*. PhD thesis, The University of Texas at Austin, May 1994.

[42] Frank P. Incropera and David P. DeWitt. *Fundamentals of heat and mass transfer*. Wiley, third edition edition, 1990.

[43] Manuel R. Conde. Aqueous solutions of lithium and calcium chlorides: Property formulations for use in air conditioning equipment design. M. Conde Engineering, Zurich Switzerland, 2004.

[44] Manuel R. Conde. Properties of aqueous solutions of lithium and calcium chlorides: formulations for use in air conditioning equipment design. *Int. J. Thermal Sci.*, 43(4):367–382, 2004.

[45] A.K. Singh, Harpal Singh, S.P. Singh, and R.L. Sawhney. Numerical calculations of psychrometric properties on a calculator. *Building and Enviroment*, 37:415–419, 2002.

[46] S.V. Patankar. *Numerical Heat Transfer and Fluid Flow*. Hemisphere, Washington, 1980.

[47] Steven C. Chapra and Raymond P. Canale. *Numerical Methods for Engineers*. Mc Graw Hill, 1998.